ACS Energy LETTERS

http://pubs.acs.org/journal/aelccp

REVIEW

Beyond Composition: Surface Reactivity and Structural Arrangement of the Cathode–Electrolyte Interphase

Julia C. Hestenes and Lauren E. Marbella*

Cite This: *ACS Energy Lett.* 2023, 8, 4572–4596

Read Online

ACCESS | Metrics & More | Article Recommendations

ABSTRACT: The role of the cathode–electrolyte interphase (CEI) on battery performance has been historically overlooked due to the anodic stability of carbonate-based electrolytes used in Li-ion batteries. Yet, over the past few decades, degradation in device lifetime has been attributed to cathode surface reactivity, ion transport at the cathode/electrolyte interface, and structural transformations that occur at the cathode surface. In this review, we highlight recent progress in analytical techniques that have facilitated these insights and elucidated not only the CEI composition but also the spatial distribution of electrolyte decomposition products in the CEI as well as cathode-driven reactions that occur during battery operation. With a deeper understanding of the CEI and the processes that lead to its formation, these advanced characterization tools can unlock routes to mitigate impedance rise, particle cracking, transition metal dissolution, and electrolyte consumption, ultimately enabling longer lasting, safer batteries.

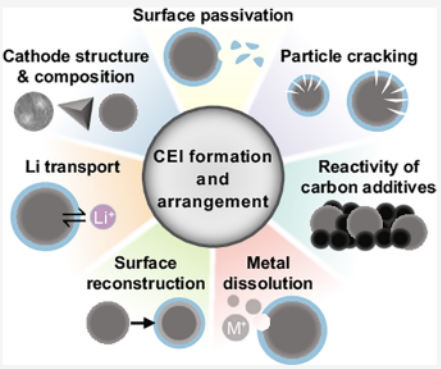

1. INTRODUCTION

The global transition to electrified transportation and intermittent sources of grid energy requires cheap, sustainable Li-based batteries with high energy and power densities.[1,2] To achieve these goals, we need to understand and control degradation in batteries with cathode materials that use widely abundant and inexpensive elements while maintaining high energy density (this is why there is a major push to eliminate cobalt from commercial Li-ion batteries (LIBs)[3]). To this end, there are four major classes of materials that minimize our reliance on cobalt: Ni-rich ($LiNi_xMn_yCo_zO_2$ (NMCXYZ, $x = 1 - y - z \geq 0.8$)) and Li-rich layered transition metal oxides ($Li_{1+x}Ni_yMn_zCo_{1-x-y-z}O_2$, Li_2MnO_3), Mn-rich spinels ($LiMn_2O_4$ (LMO), $LiNi_{0.5}Mn_{1.5}O_4$ (LNMO)), and Fe-based olivine materials ($LiFePO_4$ (LFP)). These cathodes use little (<10%) to no Co in the active particles. However, all of these materials exhibit structural and interfacial instabilities during electrochemical cycling, resulting in insufficient lifetime and safety needed for addressing long-term climate goals.[1,4,5] Specific examples of surface instability in these systems include oxygen evolution,[6−8] crystallographic reconstruction at the particle surface that changes the Li (de)intercalation behavior,[9−14] cracking of secondary particles,[15−20] transition metal dissolution,[16,21−24] and continuous electrolyte decomposition during cycling in organic solvents.[25−30] Once degradation at the cathode begins, it manifests as capacity loss, impedance rise, and thermal instability.[15,16,26,31] In addition, decomposition products from reactions between the cathode and the electrolyte form a cathode–electrolyte interphase (CEI) that alters Li transport as well as other properties of the composite film, such as binder swelling and electronic conductivity.[32−38]

The influence of the CEI on battery performance has only recently been recognized. This distinctly differs from the surface chemistry on the anode side of the battery, which has traditionally been correlated with battery degradation. Conventional carbonate solvents used in LIBs are not thermodynamically stable <1.3 V,[39] so electrochemical reduction products deposit on anodes of interest such as graphite, Li, and Si to form a ≥10 nm thick interphase coined the solid–electrolyte interphase (SEI).[40] For anodes like Li and Si that undergo a large volume change during electrochemical cycling, this SEI tends to crack and expose a fresh surface where the SEI can

Received: July 26, 2023
Accepted: September 19, 2023
Published: October 10, 2023

https://doi.org/10.1021/acsenergylett.3c01529
ACS Energy Lett. 2023, 8, 4572–4596

continue to grow and become more tortuous, impeding Li-ion transport and exacerbating capacity fade.[41−48] Conversely, these same electrolytes are electrochemically stable up to 4.5 V, which is well above the upper cutoff voltage used for most cathode materials including $LiCoO_2$ (LCO), NMC, and LFP. Therefore, no low- to moderate-voltage cathodes are expected to exhibit a CEI.

Nonetheless, evidence of the CEI was observed by Goodenough and co-workers in 1985 when they noted changes in the interfacial resistance of $Li_{1-x}CoO_2$ ($0 < x < 0.5$) as a function of state-of-charge (SOC).[49] These changes in resistance were linked to a ∼3 nm thick amorphous layer observed on the surface of a delithiated $Li_{0.1}CoO_2$ particle with transmission electron microscopy (TEM). The authors speculated that when $x \geq 0.35$ in $Li_{1-x}CoO_2$, Co^{4+} oxidized the propylene carbonate (PC) solvent to form a polymer shell around the active particles. Over the next two decades, several groups used spectroscopic methods (e.g., Fourier transform infrared (FTIR) spectroscopy, X-ray photoelectron spectroscopy (XPS)) to characterize the chemical composition of the CEI on a wide range of cathode materials, including LFP, LCO, $LiNiO_2$ (LNO), LMO, and the NMC series.[33,34,50−53] For the layered oxides, ethylene carbonate (EC) solvent decomposition starts at ∼50% SOC[26,29,54−57] and continues after chemical oxidation from reaction with evolved O_2 from the lattice (onset at ∼65−82% SOC, depending on composition),[26,29,56−63] leading to a variety of carboxylic acids, vinyl species, alcohols, and polymers in the CEI. The CEI also exhibits native Li_2CO_3 derived from exposure to atmosphere that releases CO_2 upon charge.[61,64,65] Protons generated from solvent oxidation accelerate PF_6^- decomposition, leading to insoluble phosphorus- and fluorine-containing compounds (e.g., metal fluorides, $P_xO_yF_z$) upon cycling in $LiPF_6$ salt.[22,57,66−68] The resulting CEI is also dynamic in nature; carbonate- and metal fluoride-containing CEIs can decompose or dissolve at high voltages,[69−73] and soluble species formed at the anode can migrate to the cathode during cell discharge, a phenomenon known as "anode−cathode crosstalk".[73−75]

When compared to the anode SEI, the CEI is substantially more difficult to characterize. Lower quantities of surface species and oxidation products require analytical tools with superior sensitivity and chemical resolution to distinguish from the bulk electrode and electrolyte.

Yet, how these reaction byproducts can be arranged to form a functional CEI is still not well understood. When compared to the anode SEI, the CEI is substantially more difficult to characterize. First, the CEI is typically much thinner than the SEI, likely due to the fact that the anodic stability of carbonate solvents leads to less electrolyte decomposition.[5,41,76] Lower quantities of surface species and oxidation products require analytical tools with superior sensitivity and chemical resolution to distinguish from the bulk electrode and electrolyte. Second, the composition of the active material on the cathode side of the battery is more complex than the anode side. With a mixed metal oxide, there are multiple surface sites that can react with the electrolyte, such as nucleophilic oxygen atoms (e.g., Ni−O) or catalytically active metal centers (e.g., Ni^{4+}).[54,56,57,77] Emerging anodes, like Li, only involve a single element and completely eliminate the need for carbon additives, simplifying reduction reactions. During lithiation/delithiation, many cathode materials undergo surface reconstruction that will further alter surface reactivity, leading to changes in CEI formation mechanisms with cycling. In addition, crystallographic reconstruction at the particle surface is often coupled to cracking of secondary particles, where electrolyte can penetrate and form more CEI.[16,17,78,79]

Given the complex nature of the CEI, it is incredibly challenging to link basic compositional knowledge to battery degradation. In this review, we focus on state-of-the-art methodologies used to study the CEI that offer remarkable

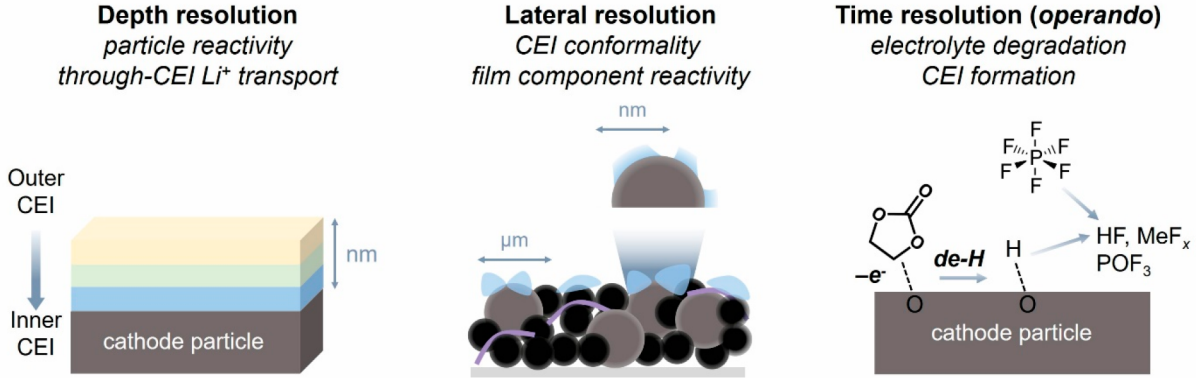

Figure 1. Different types of spatial and temporal resolution needed for characterization of the CEI structure and formation mechanisms. (Left) Methods that offer depth resolution can provide information on the origin of CEI species (and thus particle reactivity) and as well as the relative location of electrolyte decomposition products, offering information on Li^+ conductivity barriers. (Center) Micrometer-scale lateral resolution is needed to probe CEI (blue) conformality and its distribution on the composite film, providing insight on the reactivity of each individual film component, such as active particles (gray), conductive carbon (black), and binder (purple). Nanometer-scale lateral resolution is necessary for evaluating the distribution of CEI compounds across the particle surfaces. (Right) Time-resolved techniques (in situ/operando) examine the electrolyte−particle interactions that lead to CEI formation, especially processes involving transient intermediates that are difficult to detect with ex situ methods like surface-adsorbed species (e.g., surface protons, solvent fragments), acids (e.g., HF), and gases (e.g., CO_2, O_2, POF_3).

https://doi.org/10.1021/acsenergylett.3c01529
ACS Energy Lett. 2023, 8, 4572−4596

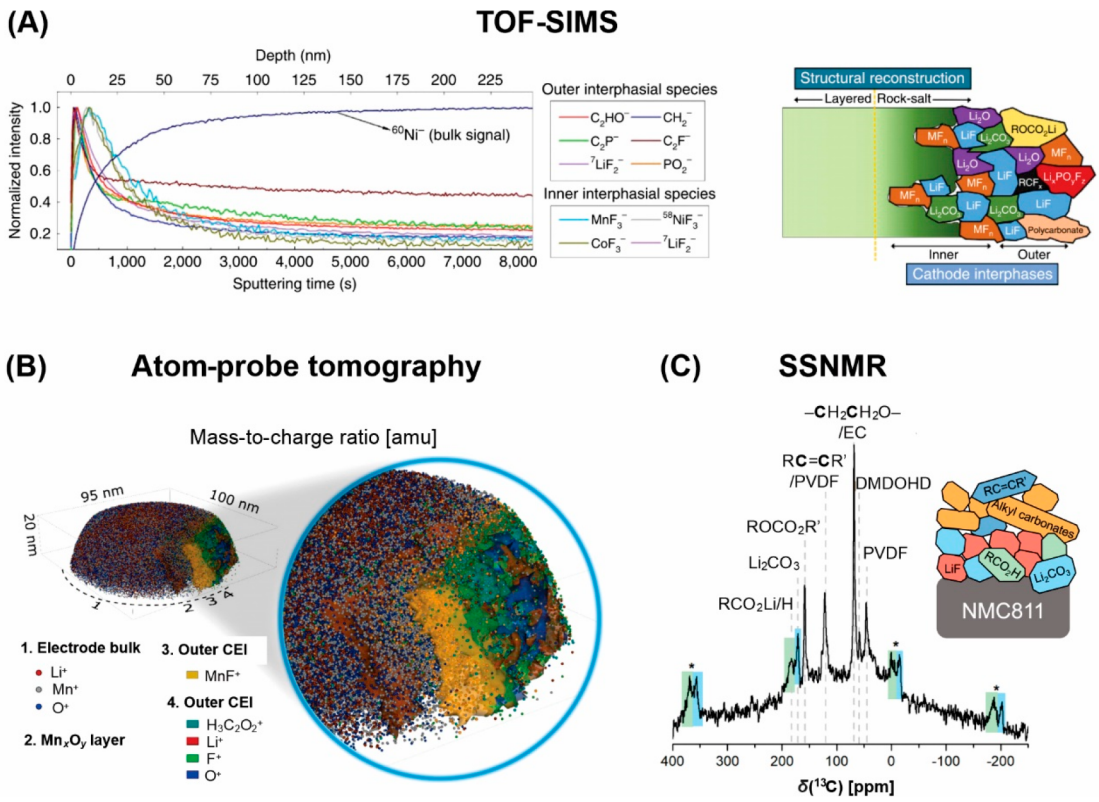

Figure 2. (A) TOF-SIMS depth profiling of secondary ion fragments from a cycled $LiNi_{0.7}Mn_{0.15}Co_{0.15}O_2$ cathode, and a representative schematic of the radial arrangement of CEI species on the particle surface. Reprinted with permission from ref 22. Copyright 2017 Springer Nature. (B) 3D ion map generated by APT of the CEI on $LiMn_2O_4$ after holding at open-circuit voltage for 240 h. Ions detected in regions 1 and 2 are depicted as spheres, while the CEI species (regions 3 and 4) are shown as solid layers. Adapted with permission from ref 99. Copyright 2020 Elsevier. (C) ^{13}C SSNMR spectroscopy of an NMC811 cathode film that underwent 50 galvanostatic cycles showing carbon-containing components in the CEI. Based on spinning sideband analysis from the paramagnetic cathode surface (marked with asterisks), Li_2CO_3 and carboxy-containing CEI species are within ~1 nm of the particle surface in the inner CEI; vinyl compounds and alkyl carbonates are found in the outer CEI. Adapted with permission from ref 55. Copyright 2021 American Chemical Society.

chemical *and* spatial or temporal (e.g., in situ/operando) resolution (Figure 1), shedding light on how the surface structure and reactivity is related to the performance. Specifically, we discuss characterization methods that offer molecular information (from the elemental properties or mass of the light elements) on the CEI generated in nonaqueous liquid electrolytes for technologically relevant cathode materials that can be performed in a distance- and/or time-resolved manner (note that several excellent reviews provide a comprehensive overview of the individual characterization techniques that have been employed to study CEI composition[41,76,80−82]). In section 2, we discuss chemical probes that yield depth information to pinpoint the precise location of individual compounds in the CEI from the cathode surface to the CEI/electrolyte interface. Section 3 focuses on imaging-based techniques that offer lateral resolution to determine where electrolyte decomposition products are located on the cathode composite (on the active particles versus the carbon additives) to understand the reactivity of each film component and how the CEI impacts the composite properties. In section 4, we cover advanced characterization techniques that provide both high chemical and temporal resolution to elucidate (electro)chemical decomposition pathways for both electrolyte salt and solvent molecules. Equipped with this insight on the surface reactivity and the structural arrangement of the CEI, we address how these cutting-edge analytical tools can help answer the following questions regarding cathode-based degradation in LIBs.

(i) What are the chemical compounds in the CEI that impede Li intercalation/deintercalation?
(ii) Do distinct parasitic reactions occur on different surface structures/compositions that require unique solutions for each cathode type?
(iii) What is the mechanism underpinning transition metal dissolution from the cathode, and what are the tools that we can use to prevent it?
(iv) What role does electrolyte oxidation play in the crystallographic reconstruction observed at the surface of cathode active particles?
(v) How does the CEI affect particle cracking, which is typically thought of as a bulk phenomenon?
(vi) How stable is the CEI in terms of dissolution and adhesion to the cathode surface?
(vii) What roles do other battery components (e.g., conductive carbon, binders) and surface species (e.g., native surface compounds) play in CEI formation and its final properties?

2. PROFILING THE CEI STRUCTURE FROM THE CATHODE SURFACE TO THE ELECTROLYTE

The arrangement of the CEI from the solid cathode film to the liquid electrolyte dictates Li^+ intercalation in and out of the

https://doi.org/10.1021/acsenergylett.3c01529
ACS Energy Lett. 2023, 8, 4572−4596

active particle. For example, metal fluorides in the inner CEI (i.e., closest to the inorganic active material) are associated with increased resistance due to their poor ionic conductivity. Transient organic components in the outer CEI that move from the anode to the cathode during cycling may also lead to cycle-to-cycle changes in resistance during lithiation/delithiation but fail to protect reactive sites on the surface.

How do we get information on the exact location of discrete CEI components? XPS is one of the most common tools for characterizing interphase chemistry on electrode surfaces. Most ultrahigh-vacuum (UHV) XPS instruments are equipped with an Ar sputtering gun that enables spectral acquisition as a function of sputtering depth to understand the structural arrangement of the CEI from the outermost surface of the CEI (i.e., closest to the electrolyte, collected before sputtering) to the innermost surface (i.e., closest to the cathode film, collected after sputtering).[33,53] In addition to XPS, time-of-flight secondary ion mass spectrometry (TOF-SIMS) is another UHV technique that offers better chemical and depth resolution. Given the ubiquitous nature of XPS and the improved chemical resolution provided by TOF-SIMS, this section will only focus on TOF-SIMS out of the two techniques. In addition, we also describe two other techniques, atom-probe tomography (APT) and solid-state nuclear magnetic resonance (SSNMR) spectroscopies, that also provide depth resolution of the CEI, offering insight into particle reactivity and barriers to Li intercalation.

2.1. Time-of-Flight Secondary Ion Mass Spectrometry (TOF-SIMS). In time-of-flight secondary ion mass spectrometry (TOF-SIMS), a focused ion beam is used to eject secondary ions from the outermost layer of the sample surface. These secondary ions (which are comprised of molecular fragments from the surface) are accelerated and separated based on their mass-to-charge ratio (m/z) and detected using a mass spectrometer. The m/z value and the peak intensity in the mass spectrum correspond to the identity and the quantity of a specific ion fragment. When evaluating the CEI composition, TOF-SIMS offers atomic-level surface sensitivity (probes a depth of <1 nm via detection of sputtered ion fragments) and exceptional elemental sensitivity (0.01−0.1% elemental concentration) and can be paired with high-resolution rastering, providing elemental images with a lateral resolution of ∼200 nm (this will be discussed in the next section).[22,30,79,83−87] These capabilities are distinct from XPS, which probes ∼2 nm deep (determined by the escape depth of the photoelectrons) and requires >0.1% elemental concentration for detection.[22,83] Similar to XPS, a sputter gun is used for depth profiling.

In 2017, Manthiram and co-workers constructed a mosaic model for the arrangement of the CEI on Ni-rich $LiNi_{0.7}Co_{0.15}Mn_{0.15}O_2$ upon cycling in 1 M $LiPF_6$ in ethylene carbonate/diethyl carbonate (EC/DEC, 1:1 v/v) based on TOF-SIMS depth profiling measurements (Figure 2A).[22] The authors discovered carbonate fragments and $Li_xPO_yF_z$ electrolyte decomposition species in the outer CEI and insoluble species like transition metal fluorides and Li_2CO_3 in the inner CEI. In this experiment, LiF was found randomly deposited in both the inner and the outer portion, which points to a mosaic CEI rather than a multilayer architecture. We expect that a mosaic CEI structure causes nonuniform Li flux to the particle surface since Li^+ transport through different CEI phases is likely disparate. These findings are similar to an earlier TOF-SIMS study, where Kim and co-workers used depth profiling to sputter away organic decomposition products in the outer CEI on the surface of LNMO after cycling and storing in a comparable electrolyte (1 M $LiPF_6$ in EC/DEC, 1:2 v/v).[30] On the inner CEI, the authors found metal fluorides like MnF_2, NiF_2, and LiF. These data indicate that layered and spinel cathodes that are susceptible to transition metal dissolution in HF-forming electrolytes (like $LiPF_6$) are likely to be coated with resistive CEI compounds.

Manthiram and co-workers also investigated the initial CEI that spontaneously forms upon soaking cathodes with different amounts of carbon black (from 1 to 10 wt %) in electrolyte. TOF-SIMS spectra collected after 30 days of aging showed that both the active particles and the carbon black chemically react with acidic species (e.g., HF) present in the electrolyte. Films with high carbon contents (10 wt %) were linked to increased C_2F^- and C_3OF^- species, which heavily coated the carbon black region and, to a lesser extent, the active particles. Meanwhile, samples with higher quantities of active particles (1 wt % carbon) showed significantly more LiF and MnF_2 compared to the 10 wt % carbon sample and are derived from acid etching of the active particle. These fragments were also detected on the carbon/binder regions (in much smaller quantities), which the authors claim was due to migration during aging. These results indicate that tuning the carbon content or secondary particle size changes the amount of ionically insulating compounds, such as metal fluorides, on the active particle surface that form upon exposure to the electrolyte. However, it is not clear if lower surface area particles prevent these metal fluorides from forming or if degradation products formed at the carbon surface (e.g., C_2F^- and C_3OF^-) serve to protect against transition metal leaching. In order to decipher how carbon additives impact the CEI structure, the role of different conductive carbons (e.g., nanostructured carbon, carbon fiber, high surface area carbon) and polymeric binders (e.g., those used in wet and dry coating) needs to be examined in more detail. These studies should preferably be performed in conjunction with characterization methods that do not require sample rinsing that can alter the placement of CEI species, given that each component is expected to exhibit unique surface chemistry. Further, the boundary between carbon additives and active particles may be more reactive than either component alone, presenting additional challenges in studying local changes in composites and thus presents the need to use techniques, like TOF-SIMS, that offer additional lateral resolution (see the next section).

Moving beyond conventional carbonates, Peng and co-workers used TOF-SIMS to examine the CEI formed upon cycling NMC111 (for 100 cycles) in 1 M $LiPF_6$ in EC/DMC/EMC (1:1:1 by weight) in the coadditive solution containing 1 wt % $LiPO_2F_2$ and 10 wt % fluoroethylene carbonate (FEC).[84] The additive-containing electrolyte improved capacity retention after 400 cycles by about 200% compared to the baseline electrolyte. TEM images show that the baseline electrolyte (no additive) generated a 24 nm thick CEI, while the CEI formed in the presence of coadditives was only 6.8 nm thick, indicating that the additive helped form a passivating layer that mitigated electrolyte decomposition/CEI growth in long-term cycling. TOF-SIMS of both the baseline and the additive-containing electrolyte showed that the outer CEI is comprised of organic species (CH_2^-, C_2HO^-, C_2P^-, C_3P^-, C_3F^-), $Li_xPO_yF_x$, and Li_2CO_3, while the inner CEI is comprised of transition metal fluorides and oxides. LiF distributes in both the inner and the outer CEI. LiF, C_2P^-, C_3P^-, and $Li_xPO_yF_x$ were detected in

https://doi.org/10.1021/acsenergylett.3c01529
ACS Energy Lett. 2023, 8, 4572−4596

relatively higher quantities in the FEC/$LiPO_2F_2$-containing electrolyte. There were also fewer organic species and transition metal fluorides in the CEI when additives were present compared to the control, indicating that both solvent oxidation and salt decomposition (which forms HF and transition metal fluorides) were mitigated upon addition of the additives. Together, the findings from TOF-SIMS and TEM indicate that the thin, dense LiF-rich (although the function of LiF is not entirely clear, vide infra) CEI formed by the FEC/$LiPO_2F_2$ additives prevented decomposition of the organic solvents, $LiPF_6$ salt, and dissolution of the transition metals. These results agree with separate literature that reports the addition of FEC to a $LiPO_2F_2$-containing carbonate electrolyte increases the quantity of fluorine content in both the CEI and the SEI, which results in better cycle life in NMC532/graphite pouch cells and reduced parasitic heat flow during cycling.[88]

There are a few routes that these coadditives may alter the CEI and enhance LIB performance. For example, excess $LiPO_2F_2$ at the particle surface could shift the equilibrium of salt hydrolysis in favor of the reactants, preventing $LiPF_6$ breakdown,[25] ultimately minimizing the amount of HF formation and transition metal leaching. A LiF-rich CEI is often correlated with improved cycle life, but the origin of LiF and its role is not well understood since it is randomly dispersed throughout the inner and outer CEI and is a relatively poor ion conductor.[89] Given the high oxidative stability of FEC, the increased quantity of LiF in the CEI may arise from the reductive defluorination at the anode, where LiF is produced and then later transferred to the CEI through crosstalk. Another byproduct of FEC reduction is poly(vinylene carbonate) (poly(VC)), which may also move to the cathode surface, where it passivates the surface and prevents mechanical degradation of the NMC secondary particles.[17,20] Additional work to elucidate the source of organic fragments in the outer CEI with TOF-SIMS through experimental strategies, such as isotopic labeling of small molecules, can help parse the role of different additives on the CEI structure and functionality.

Overall, the spatial resolution and chemical sensitivity of TOF-SIMS as well as its accessibility (laboratory based) make the technique an important tool for CEI characterization, although we do note that many institutions are more likely to have access to an XPS than a TOF-SIMS instrument. TOF-SIMS offers deeper insight into the molecular structures, particularly for light elements (present in both the organic and the inorganic CEI), compared to X-ray-based techniques while still maintaining information on the radial arrangement. For example, TOF-SIMS can resolve the different types of metal fluorides that form upon cycling mixed metal oxide cathodes (e.g., LiF, MnF_x, and NiF_x),[30,86] a task that is much more challenging with XPS due to overlap in the F 1s orbital. In section 3.2, we also discuss the utility of TOF-SIMS for imaging the lateral distribution of chemical compounds in the CEI, making it a versatile tool to characterize the CEI in three dimensions. However, for TOF-SIMS, the user relies on detecting ion fragments as well as sputtering to obtain a depth profile, which may result in damage to the CEI, particularly for reactive solvent decomposition species. As with other UHV methods, rinsing during sample preparation to prevent charging may alter the CEI and/or remove soluble species.

2.2. Solid-State Nuclear Magnetic Resonance (SSNMR) Spectroscopy. In nuclear magnetic resonance (NMR) spectroscopy, the sample is placed in a strong magnetic field and irradiated with radiofrequency (rf) pulses to excite NMR-active nuclei. The energy released from nuclear spin relaxation is detected to produce an NMR spectrum with peaks at distinct frequencies that depend on the local electronic structure as well as the dynamics in the system. As a result, NMR enables precise assignment of molecular structures and interactions between different components in the CEI. Therefore, solid-state NMR (SSNMR) spectroscopy provides a sensitive readout of the different types of organic molecules, inorganic compounds, and functional groups as well as their interactions in the CEI.

For instance, Dupré and co-workers used SSNMR spectroscopy to examine the dynamics of the CEI during battery operation for LFP and $LiMn_{0.5}Ni_{0.5}O_2$ using ^7Li, ^{19}F, and ^1H SSNMR spectroscopies.[75,90] In both of these studies, the authors found evidence of anode−cathode crosstalk (the movement of interphase compounds from the anode to the cathode during discharge/charge) when the NMR resonance corresponding to the CEI (e.g., LiF) would increase in intensity at discharge but decrease at charge. These reports also showed that the NMR spectra of CEI species attached to strongly paramagnetic cathode materials are broadened due to nuclear coupling to nearby unpaired electrons[91,92] (nearly all technologically relevant cathode materials are strongly paramagnetic). This broadening can provide an advantage and a disadvantage; on one hand, it offers distance-dependent information on where certain compounds are located in the CEI, but it may obscure differentiation of overlapping resonances if it is too severe.

We were able to obtain high-resolution structural information on the CEI of select cathode materials by intentionally manipulating the paramagnetism of the active material either through material choice or electrochemistry. In the first example, we used Li_2RuO_3 as a model compound to study the CEI composition and anode−cathode crosstalk after cycling in 1 M $LiPF_6$ in EC/DMC[93] because it has substantially lower paramagnetism than other cathodes but retains the degradation processes common to layered Li-rich materials (e.g., oxygen evolution). Using surface-sensitive dynamic nuclear polarization (DNP) NMR spectroscopy, we identified several different organic components in the CEI, including poly(ethylene oxide) (PEO)-type polymers, alkyl carbonates, and Li salts, on Li_2RuO_3 after just one cycle.[93] The composition of the CEI remained nearly identical between the 1st cycle and the 100th cycle, indicating that the cathode decomposition processes that occur in cycle 1 dictate the electrolyte decomposition. In Li_2RuO_3, most oxygen is evolved in the first cycle,[94] where it can attack the carbonate solvent; the resulting decomposition products then deposit on the cathode surface. By comparing the spectra acquired on charge and discharge, we see that Li-coordinating small molecules in the outer CEI (e.g., acetate, small oligomers) desorb during delithiation but are reversibly redeposited during the subsequent lithiation step likely due to crosstalk.

In separate work, we took advantage of the fact that upon charging NMC811 to 4.6 V, most of the paramagnetic Ni^{2+} is oxidized to diamagnetic Ni^{4+} to produce a material that is less paramagnetic than its fully lithiated counterpart and that can be used to study the CEI formed on NMC811 with high-resolution, magic-angle spinning (MAS) SSNMR spectroscopy.[55] Since the active particle is still paramagnetic (e.g., due to Mn^{4+} centers and reduction that occurs during surface reconstruction), CEI compounds closest to the delithiated

https://doi.org/10.1021/acsenergylett.3c01529
ACS Energy Lett. 2023, 8, 4572−4596

NMC811 surface will still experience line broadening (as noted above). When spinning a sample that contains a paramagnetically broadened NMR line at the magic angle, the broad peak will split into a spinning sideband pattern that contains multiple peaks. The spinning sideband manifold contains the isotropic resonance (that corresponds to a specific functional moiety) surrounded by sidebands that appear at integer units of the MAS frequency. This discretization of the broad NMR peak allows the user to assign the chemical shift for each CEI component and determines which species is closest to the paramagnetic cathode surface. (This line broadening effect is distance dependent, so CEI compounds far away from the particle surface will only show an isotropic resonance with no spinning sideband pattern.) From this analysis, we found that the carbon-containing CEI on NMC811 produced after 50 cycles in 1 M $LiPF_6$ in EC/DMC contained Li_2CO_3 and Li acetate/oxalate within 1 nm of the particle surface (Figure 2C). Other species observed in ^{13}C SSNMR spectroscopy (e.g., alkyl carbonates/esters and vinyl compounds) do not exhibit spinning sidebands, indicating these species are >1 nm from the active particle. The exact location on the composite is difficult to decipher with this technique, but it could be inferred that these compounds are either on the outer radius of the CEI deposited on the active particle itself and/or on the carbon additives. Our study paired these experiments with a laterally resolved microscopy technique (XPEEM, see section 3.3), which supported that these CEI components are distributed on the entire composite surface. In situ ^1H solution NMR spectroscopy (vide infra) also detected the presence of vinyl compounds, indicating that these species are soluble and may desorb from the surface and redeposit on either the particle or the carbon additives. There is a growing body of evidence indicating that the presence of these Li alkyl carbonates and vinyl species is correlated with increased impedance in LIBs that use Ni-rich cathodes.

SSNMR spectroscopy is a potentially powerful tool to address how organic compounds, in particular, may impact the interfacial properties in LIB cathodes. However, one drawback of using SSNMR spectroscopy for depth probing is that high-resolution structural assignment strongly depends on the magnetic properties of the bulk cathode material. Therefore, examination of the organic CEI with SSNMR spectroscopy is most likely applicable to Ni-rich compounds with $Ni^{2+/4+}$ redox chemistry, such as NMC811, $LiNi_{0.8}Co_{0.15}Al_{0.05}O_2$ (NCA), and/or $LiNiO_2$ (LNO) at high voltage, and can be used to systematically evaluate the impact of electrolyte additives and cycling protocols within those systems. Further, many CEI species themselves are paramagnetic and are not easily detected with SSNMR spectroscopy, like transition metal fluorides, so studies should be complemented with other techniques to gain a full understanding of the CEI composition. In general, SSNMR spectroscopy is a non-destructive bulk analytical technique (no exposure to electron/X-ray beams, UHV, or sputtering) that can be carried out in air-free conditions and is readily available at many research institutions. Although the methods described above are performed postmortem, samples can be prepared in such a way that they closely resemble or minimally disturb their native environment (e.g., sample rinsing/drying is not needed; the cathode sample can even be packed with liquid electrolyte and separator[95]).

2.3. Atom-Probe Tomography (APT). In atom-probe tomography (APT), an electric field is used to evaporate ions from a conical sample tip (radius of ∼100 nm) under UHV at cryogenic temperatures. The evaporated ions are collected onto a position-sensitive TOF-MS. The m/z ratio in the mass spectrum coupled with the position data enables reconstruction of a three-dimensional (3D) compositional map of individual compounds in the CEI.

Until recently, APT had only been used to study the structure of the bulk cathode particle itself.[96−98] In 2020, Scipioni et al. used APT to generate a 3D elemental map of the CEI that forms at open-circuit voltage (OCV) on a single LMO particle after aging for 240 h in 1 M $LiPF_6$ in EC:DMC (1:1 v/v) (Figure 2B).[99] The structures generated with APT showed homogeneous inner layers of MnF_x stacked on top of Mn_xO_y and an outer layer containing a mixture of LiF, Li_2O, and polycarbonates from chemically-driven electrolyte decomposition (Figure 2B). The authors were also able to quantitatively plot how CEI composition changed as a function of depth, moving from the outer to the inner CEI.

Time-resolved electrochemical impedance spectroscopy (EIS) showed an increase in charge-transfer resistance in the first 24 h of aging, which the authors attributed to the formation of manganese fluoride from reaction between the particle and trace HF, which has a lower electronic conductivity than LMO. The authors attributed the gradual increase in charge-transfer resistance over 240 h to the deposition of organic and inorganic compounds on the cathode surface. These EIS findings suggest that transition metal fluorides are resistive species that impede Li-ion intercalation/deintercalation, which is consistent with their bulk properties. The findings on CEI arrangement agree with those from TOF-SIMS and XPS[30,33,100] while providing a compelling visualization of an intact CEI. Moving forward with detailed chemical mapping, we can more rationally fit ambiguous EIS data with the appropriate equivalent circuit that accurately describes the electrochemical behavior.

Unfortunately, APT is complex and requires highly specialized equipment. Sample preparation is nontrivial—it requires a needle-shaped sample with an apex diameter of 10−100 nm, which is obtained by focused-ion beam (FIB) milling from the cathode, which may disrupt the CEI. Since the measurement probes only a very small portion (few nanometers) of the cathode, the sample may not be representative of the entire surface. Despite these challenges, APT has the unique ability to map both heavy and light elements with high chemical sensitivity (0.01−0.1% elemental concentration) and subnanometer resolution (∼0.2−0.5 nm), making the technique one of the highest resolution characterization techniques accessible for CEI studies.[101]

2.4. Insights into the CEI Gained from Depth-Resolved Techniques. Most methods that provide depth resolution on the order of nanometers or subnanometers agree that inorganic metal fluorides (LiF, MnF_2, NiF_2) and carbonates (Li_2CO_3) lead to lower ionic and electronic conductivity and are often concentrated in the inner CEI for Li- and Mn-rich cathodes.[22,30,99] Organic species, Li alkyl carbonates, and other more soluble electrolyte decomposition species (which can include metal fluorides that are dissolved at high voltage when local HF concentrations are high) are often found in the outer CEI.[76,99] The effect of these organic components on the ionic and electronic conductivities of the CEI is still less understood, and comparing the ionic conductivities of each CEI component (transition metal fluorides, LiF, alkyl carbonates, polymers, etc.) can help

https://doi.org/10.1021/acsenergylett.3c01529
ACS Energy Lett. 2023, 8, 4572−4596

inform CEI design beyond what is currently known for bulk inorganic compounds. In addition, it is possible that the organic CEI imparts flexibility at the surface to prevent particle cracking and electrolyte consumption, but in order for this to happen, it must remain attached to the particle surface. All of the aforementioned methods can, in principle, quantify organic species in the CEI and can establish their role in battery performance.

An understanding of the structural arrangement of the CEI across different cathode materials can also provide insight into reactivity. While fewer reports provide depth information on the CEI for Li-rich structures, intuition suggests that it may be similar to that observed for Ni-rich cathodes. Since Li-rich cathodes tend to evolve more O_2,[59,93,100,102] we expect that these CEIs may exhibit higher quantities of polymeric structures, further emphasizing the need for more detail on the organic portion of the CEI. In high-voltage cathode materials, the CEI is not stable above 4.5 V vs Li/Li^+ due to the highly acidic environment that dissolves the CEI, highlighting the dynamic nature of these structures.[68,69,72] For all cathode compositions, the apparent concentration and location of all of the CEI components appear to depend on whether the cell is analyzed at charge or discharge due to anode−cathode crosstalk, and this should be taken into consideration before drawing conclusions. Finally, due to its low operating voltage, LFP has not been explicitly mentioned above because it is believed to form a relatively thin CEI layer in typical carbonate solvents based on XPS and TOF-SIMS.[33,103] The literature consensus at this time is that the CEI on LFP is relatively homogeneous and predominantly salt derived.[33,103] To the best of our knowledge, no Fe_xF_y species have been detected on the surface of LFP under typical cycling conditions,[104,105] although further investigation is warranted.

For all cathode compositions, the apparent concentration and location of all CEI components appears to depend on whether the cell is analyzed at charge or discharge due to anode−cathode crosstalk, and this should be taken into consideration before drawing conclusions.

For all cathode materials, a thick, mosaic CEI on the active material as well as the presence of species that dissolve or diffuse away are undesirable. Instead, a compact, multilayered CEI that does not react away (through either crosstalk or acid dissolution) would allow consistent Li transport and prevent impedance buildup over time. Achieving this requires an electrolyte that, upon oxidation, forms a passivating CEI on the particle and is (electro)chemically resistant to further degradation. Several strategies exist to improve performance in this realm, such as coating the cathode and/or optimizing the electrolyte.[106,107] Yet, how these approaches alter the radial arrangement of the CEI (beyond adding a coating, for example) is still not well understood and will require concerted effort of multiple characterization techniques as CEI thickness is reduced to sub-3 nm and exhibits only short-range order.

3. LATERAL RESOLUTION OF THE CEI ACROSS THE COMPOSITE CATHODE FILM

Most cathode films are composites that contain high surface area conductive carbons and polymeric binder in addition to the active particles. Understanding CEI conformality and its deposition on active particles and carbon additives is required to identify the formation reactions at play during cycling and the functional properties of the CEI, such as ionic and electronic conductivity. Therefore, surface characterization tools equipped with lateral resolution are required to parse the role of all film components within the CEI. Since cathode active particles are usually between 1 and 30 μm (LNMO and LFP particle size is ∼5 μm, NMC811 and NCA secondary particles are around ∼10−30 μm, while primary particles are ∼200−1000 nm), we must be able to probe the lateral CEI composition at submicrometer levels to distinguish the carbon additives from the active material.

3.1. Transmission Electron Microscopy (TEM). Transmission electron microscopy (TEM) passes an electron beam through an ultrathin (<100 nm) sample (e.g., electrode particles suspended on a grid) to produce a highly magnified image after interacting with the sample. High-resolution (<0.2 nm) images are captured due to the short wavelength of electrons compared to light. Although standard sample preparation methods and accelerating voltages used in conventional high-resolution (HR) TEM may compromise the CEI,[108] advances in cryo-TEM (typically used to study sensitive biological samples) sample preparation have been used to preserve the surface structure of battery electrodes under cryogenic temperature, reduce reactivity with the electron beam through lower doses, and protect the sample from air.[24,108,109]

In a traditional HRTEM study (noncryogenic), Kim and co-workers[30] found a 5 nm MnF_2 nanoparticle at the surface of LNMO extracted from a cell that was stored at 100% SOC at 60 °C for 60 days. Detection of MnF_2 on LNMO particles is consistent with observations from our laboratory using X-ray photoemission electron microscopy (XPEEM), where we see higher quantities of MnF_2 build up on the surface of spinel-type cathodes compared to layered cathodes (which predominately contain LiF) due to increased transition metal dissolution from high voltage operation.[55,68] Upon subsequent storage at high SOC, Kim and co-workers reported that LNMO will self-discharge, leading to more electrolyte oxidation and HF production. As a result, more transition metal fluorides are expected to accumulate on cathodes stored at high SOC compared to storage at lower SOC. In separate work, Xu and co-workers[109] used cryo-TEM to examine the CEI formed on LNMO cathodes after 50 cycles in a standard carbonate electrolyte (1.2 m $LiPF_6$ in EC/EMC 3:7) versus a concentrated, sulfone-based electrolyte (3 m LiFSI in sulfolane, Figure 3A).[24] Cryo-TEM images of the CEI generated in the carbonate electrolyte showed an uneven, nonconformal CEI along the surface of the active particle (Figure 3A, left). In contrast, the sulfone-based electrolyte produced a conformal CEI with a consistent thickness of ∼0.6 nm across the LNMO surface (Figure 3A, right) and extended cell lifetime from 150 cycles to 1000 cycles with 69% discharge capacity retention by the 1000th cycle. The authors proposed that the enhanced performance observed in the sulfone-derived CEI was due to the large energy barrier to gas (SO_2) generation upon ring opening of the sulfone solvent (0.93 eV),

https://doi.org/10.1021/acsenergylett.3c01529
ACS Energy Lett. 2023, 8, 4572−4596

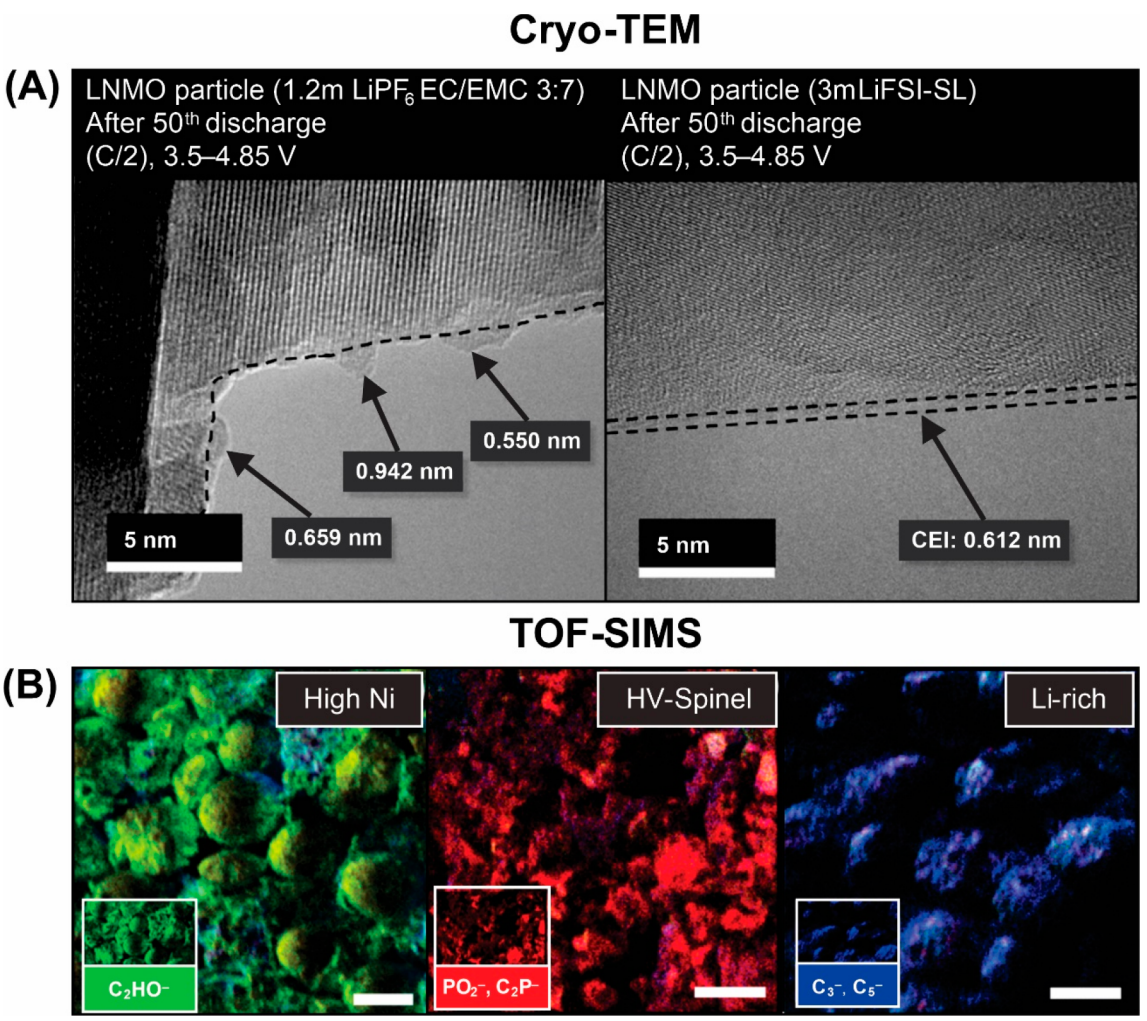

Figure 3. Characterization of the lateral deposition of the CEI. (A) Cryo-TEM images of the CEI formed on an LNMO cathode after cycling in a standard carbonate electrolyte (left) versus a carbonate-free (sulfolane-based) electrolyte, where the latter electrolyte shows a more conformal CEI that is associated with improved cycling performance. Adapted with permission from ref 24. Copyright 2018 Elsevier. (B) TOF-SIMS chemical mapping of an Ni-rich cathode ($LiNi_{0.94}Co_{0.6}O_2$), a high-voltage spinel cathode ($LiNi_{0.5}Mn_{1.5}O_4$), and a Li-rich cathode ($Li_{1.2}Ni_{0.2}Mn_{0.6}O_2$) after 115 cycles. Each image includes maps of the signal from decomposed organics in green (left), phosphates in red (middle), and polymeric carbons in blue (right). The scale bar corresponds to 10 μm. Adapted with permission from ref 100. Copyright 2020 American Chemical Society.

whereas EC is known to readily decompose into CO_2 and CO at high voltage. Instead, the sulfolane molecules were hypothesized to polymerize on the LNMO surface and form the dense, conformal CEI observed in cryo-TEM that may prevent further electrolyte decomposition. This work suggests that the decomposition of organic solvent is critical to improving the performance, and knowledge of the resulting CEI structures can be leveraged to prevent capacity fade. From the imaging analysis, we know that we will need analytical methods that can probe light elements (C, O, S) in a subnanometer CEI to fully understand the proposed mechanism.

Uneven CEI deposition is consistently correlated with poor battery performance across the board for all cathode materials, with the NMC series being some of the most studied compounds. Work by Feng, Wang, Ouyang, and co-workers on NMC811 showed that replacement of the carbonate solvent with an all-fluorinated electrolyte (1 M $LiPF_6$ in FEC:FEMC:HFE) results in a more uniform (in thickness), thinner CEI measuring ∼1.9 nm, which is correlated with increased thermal stability and less surface rocksalt reconstruction.[110] Cryo-TEM was also used to understand the cycling stability in NMC811 in ether-based electrolytes upon modifying LiTFSI (terminated by $-CF_3$ groups) to LiNFSI (terminated by $-C_4F_9$ groups), where the cycling lifetime was extended from 26 cycles to 100 cycles.[111] Analysis with cryo-TEM showed that cycling in 1 M LiNFSI in DME produces a thinner CEI of ∼5 nm compared to 1 M LiTFSI in DME, which was ∼13 nm. XPS experiments indicated that continuous CEI growth in the LiNFSI electrolyte was mitigated because of perfluoroalkane byproducts that formed a passivating CEI that ultimately extended the battery lifetime. Given these findings, examining the decomposition products generated from LiTFSI and LiNFSI with techniques that offer high chemical resolution for light elements will provide deeper insight into the exact CEI structures that impart longer cycle life.

One route to probe light elements in TEM is through the use of electron energy loss spectroscopy (EELS). For example, Cui and co-workers used EELS in cryo-EM measurements to produce elemental maps of the CEI deposited on both the

https://doi.org/10.1021/acsenergylett.3c01529
ACS Energy Lett. 2023, 8, 4572−4596

conductive carbon and the NMC532 particles after electrochemical shorting in 1 M $LiPF_6$ in EC/DEC 1:1, v/v.[108] The short circuit was used to generate a CEI on the nanoparticles after no CEI was visible in cryo-EM on nanoparticles that had undergone 100 cycles at 2.7−4.3 V, which the authors attributed to a highly heterogeneous CEI. This report demonstrates that sample preparation and sampling size (how many particles are measured) may present a challenge for CEI detection in cryo-TEM, as a CEI is certainly expected to be detected after 100 cycles on NMC811. However, they did detect a conformal CEI on the active material and carbon black particles from samples extracted from a cell that underwent 30 s of electrochemical shorting, illustrating how cryo-TEM/EELS can be leveraged to study CEI chemistry under failure conditions. In the EELS experiments on the CEI formed via shorting, the authors were able to assign some functional groups present with C K-edge measurements, but no fluorine (F K-edge) signal was detected, indicating that the shorting experiment only resulted in decomposition of the solvent rather than the salt. Accordingly, the CEI layer (∼5 nm) did not exhibit any crystalline phases in the CEI.

One of the few TEM reports on the CEI on LFP also showed that a nonconformal layer is detrimental to cell performance in terms of cycling (capacity retention and rate capability) as well as thermal stability. Wang and co-workers compared the CEI generated on the surface of LFP in 1 M $LiPF_6$ in EC/EMC vs that with 6 vol % of a fluorinated flame retardant, ethoxy (pentafluoro) cyclotriphosphazene (EPCP) with conventional TEM and TOF-SIMS.[103] For the sample cycled in the standard carbonate electrolyte, TEM showed that the thickness of the CEI varied across the surface, with regions ranging from 3−4 to 8−10 nm. Upon addition of EPCP, the CEI was smooth and approximately 2−3 nm thick. The authors propose that HF attack (due to lack of passivation) was responsible for the poor performance of LFP in the absence of any additive. In turn, the addition of EPCP prevented particle pitting and reduced the amount of ionically and electronically resistive LiF deposited on the surface of the active particles and the carbon additives. Interestingly, this finding implies that the presence of LiF in the CEI is detrimental to battery performance, which is counter to many arguments made in the literature. One distinction with this system is that LFP is less conductive than other cathode materials, making it potentially more sensitive to LiF in the CEI. These data suggest that LiF in the CEI may also actually hinder ionic and electronic transport in other cathodes as they become more resistive over the course of electrochemical cycling (e.g., due to surface reconstruction) and needs to be more critically examined, especially as the system evolves.

In addition to ex situ TEM, research efforts are also underway to develop approaches to track the nucleation and growth of CEI compounds in real time using in situ TEM. For example, Li, Li, Zeng, and co-workers used in situ TEM to visualize LiF nucleation on a patterned Ti electrode at positive potential.[112] In this work, the authors biased a symmetrical cell containing 1 M $LiPF_6$ in PC to 4 V relative to the Ti counter electrode. While precise determination of the voltage was not possible without a third reference electrode, the measurement of positive current indicated that the working electrode was inducing electrochemical oxidation events. At positive current, discrete LiF particles nucleate and grow into larger particles that can detach and disperse into the electrolyte, simulating events that may occur during battery charging. Development of this technique to enable usage of industrial electrodes and cycling protocols would be a significant breakthrough for battery interface science.

In both ex and in situ TEM, interactions between the sample and the electron beam are a concern, so cryo-TEM remains the state-of-the-art to acquire subnanometer-scale (atomic resolution) images of the CEI. The expertise to carry out cryo-TEM is commonplace at research institutions that host biomedical research, and proper sample preparation is key to achieving reproducible results. For example, submerging the sample in liquid nitrogen may alter Li surface species, whereas specialized cryoholders that can transfer the sample to the instrument under Ar may better preserve the CEI.[113] Sample rinsing prior to mounting may also impact the surface chemistry. For the CEI in particular, it can be difficult to search for and identify individual compounds in the CEI from diffraction because it tends to be very thin and amorphous (especially compared to the SEI on the anode side of the battery which can grow up to tens of nanometers),[114,115] but users may complement these measurements with EELS for chemical characterization.

3.2. TOF-SIMS. In addition to the depth profiling capabilities discussed in the previous section, TOF-SIMS also provides chemically specific maps that offer compositional information on the CEI for composite films. These maps allow us to distinguish the CEI deposited on the active particles and the carbon additives in the cathode film with lateral resolution on the order of ∼200 nm.[22,83] Manthiram and co-workers used this technique to compare the CEI compositions and layouts formed on different cathode materials: Ni-rich ($LiNi_{0.94}Co_{0.6}O_2$), Li-rich ($Li_{1.2}Ni_{0.2}Mn_{0.6}O_2$), and high-voltage spinel ($LiNi_{0.5}Mn_{1.5}O_4$) cycled in 1 M $LiPF_6$ in EC/EMC for 115 cycles (Figure 3B).[100] The resulting maps of the outer layer of these three CEIs reveal that the Ni-rich cathode surface is dominated by carbonate solvent decomposition products, the CEI on the spinel mostly contains $LiPF_6$ decomposition species, and the CEI on Li-rich materials contains high quantities of polycarbonates. The solvent degradation products found in the CEI of Ni-rich and Li-rich cathodes were attributed to the release of oxygen from the lattice, which is exacerbated in Li-rich materials, forming more polymerized species. The CEI on LNMO contained more $LiPF_6$ decomposition products (e.g., different PO_xF_y fragments) due to the high operating voltage of this material, which generates reactive protic species that decompose $LiPF_6$ salt. Note that all three maps depict outer CEI species that deposit on both the active particle as well as the carbon additives. Electrolyte solvent decomposition proceeds either via chemical oxidation reactions with evolved O_2 (in Ni- and Li-rich layered cathodes) or via electrochemical oxidation due to high-voltage cycling (spinel).

An earlier study (discussed in Figure 2A) from the same group used TOF-SIMS mapping to more closely examine CEI stability and show that, due to transition metal dissolution, transition metal fluorides are found on carbon black/binder after cycling Ni-rich layered cathode materials[22] and are consistent with other reports in the literature.[68] The instability of the transition metal fluorides implies that these species may reversibly penetrate cracks in secondary particles and lead to additional mechanical instability. To test this, Lee and co-workers used TOF-SIMS mapping to examine the filling of microcracks in secondary NMC811 particles comprised of both PEDOT-coated and uncoated primary particles.[79] In this

https://doi.org/10.1021/acsenergylett.3c01529
ACS Energy Lett. 2023, 8, 4572−4596

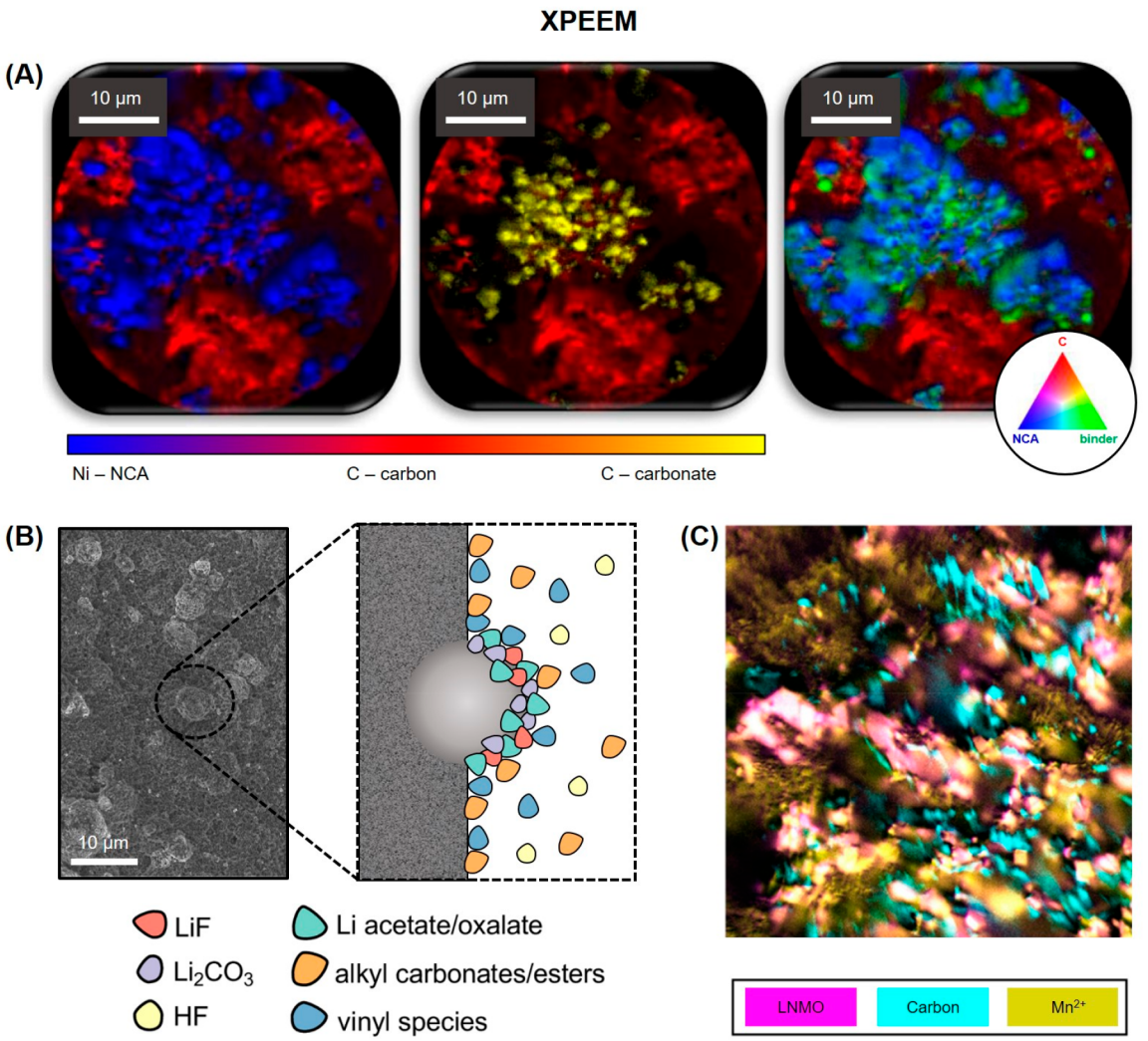

Figure 4. (A) XPEEM elemental maps of a pristine NCA ($LiNi_{0.8}Co_{0.15}Al_{0.05}O_2$) cathode, showing the active particles (blue), conductive carbon (red), binder (green), and surface carbonates in the CEI (yellow). Adapted with permission from ref 118. Copyright 2020 AIP Publishing. (B) Schematic diagram of the CEI on NMC811 after 50 cycles. XPEEM indicates that LiF is present only on the NMC particles, while soluble oligomers were detected throughout the composite film. Adapted with permission from ref 55. Copyright 2021 American Chemical Society. (C) XPEEM elemental map of an LNMO cathode film after 50 cycles, showing LNMO particles (magenta), conductive carbon (cyan), and Mn^{2+} assigned to MnF_2 (yellow). The map shows that MnF_2 deposits on both the active particles and the carbon additives. The image is of a 30 μm × 30 μm region on the cathode. Reprinted with permission from ref 68. Copyright 2022 American Chemical Society.

work, the authors found that both P- and C-based decomposition products filled the cracks that are generated in uncoated NMC samples, whereas the soft PEDOT coating likely protected the NMC surface during the lattice changes that occur during lithiation/delithiation. Even though P-containing salt decomposition products were observed in the cracks, F-containing species, like NiF_2, were only observed on the film surface. The study did not mention if the CEI was analyzed at charge or discharge, so it is difficult to know if the lack of metal fluoride in the cracks is due to dissolution. These findings underscore the importance of characterizing the CEI at SOCs where these compounds are stable so that we can understand how the surface chemistry impacts different modes of degradation (e.g., particle cracking, loss of contact[17,20]).

Although we know that high-voltage perturbation can disrupt the CEI and impact the location of the individual components, less is known regarding the distribution of the CEI on low-voltage LFP cathodes. In one study, TOF-SIMS maps reported by Wang and co-workers suggest that LFP also has a random distribution of CEI species across the composite after 150 cycles in 1 M $LiPF_6$ in EC/EMC.[103] The authors detect inorganic CEI species such as LiF, PO_3^-, and PO_2^- fragments as well as organic ion fragments from solvent decomposition like CH_3O^- and C_2^-. For composites with LFP, a large amount of carbon is typically used, making it difficult to decouple the role of CEI instability, the deposition of soluble byproducts, and additive reactivity. A comparative analysis of the CEI on LFP versus the conductive carbon matrix will help elucidate these differences in reactivity.

The lateral resolution (~200 nm) of TOF-SIMS is also helpful when evaluating CEI conformality on the micrometer scale. For example, Guo and co-workers compared the CEI formed on cycled NMC ($LiNi_{0.9}Mn_{0.04}Co_{0.06}O_2$) both with and without an amorphous coating of Li_2CO_3 (5−18 nm thick), which exhibited improved cycling performance.[87] TOF-SIMS revealed that the conformal Li_2CO_3 coating is partially

https://doi.org/10.1021/acsenergylett.3c01529
ACS Energy Lett. 2023, 8, 4572−4596

consumed during cycling to form a LiF-rich CEI which prevented particle cracking by protecting the surface, whereas the LiF formed on the uncoated NMC is unevenly distributed. Although TOF-SIMS provided some insight into the conformality, it is important to note that there are many processes that are important to battery performance that will not be captured at this lateral resolution and are perhaps better suited for TEM, such as pinholes/etching of surface coatings like Al_2O_3 by HF.[116,117]

Given that TOF-SIMS is used for both lateral mapping and depth profiling of the CEI, we direct the reader to the prior section on depth profiling for a summary of the advantages and disadvantages associated with the technique.

3.3. X-ray Photoelectron Emission Microscopy (XPEEM). X-ray photoemission electron microscopy (XPEEM) has emerged as a powerful tool for analyzing the lateral deposition of the CEI on composite cathode films.[55,118−121] XPEEM is a synchrotron-based characterization technique that produces surface-sensitive (detection depth ≈ 2−10 nm) images where intensity is proportional to the amount of soft X-ray absorption (sXAS) of the sample, typically in a 30 μm × 30 μm region on the cathode. This method combines the basic principles of sXAS and electron microscopy, where soft X-rays are used to interact with the electrons on the material surface to probe the local bonding environment and provide image contrast. The XPEEM images are acquired at discrete incremental energies, yielding an image set which offers pixel-wise XAS with a lateral resolution of ∼70−180 nm.[121] Local XAS from regions of interest (ROIs) can be extracted from the image set as well as chemically specific maps. Therefore, XPEEM can distinguish between active particles, conductive carbon, and binder as well as the CEI species that rest on top.

In recent work, El Kazzi and co-workers mapped the distribution of native carbonates on the surface of pristine Ni-rich NCA cathodes ($LiNi_{0.8}Co_{0.15}Al_{0.05}O_2$) (Figure 4A).[118] Upon charging to 4.9 V vs Li/Li^+, these residual carbonates disappear. An earlier study by the same group used XPEEM to characterize the CEI on Li-rich NMC $(Li_{1.17}Ni_{0.22}Co_{0.12}Mn_{0.66})_{0.83}O_2$, which showed surface species like C═O and Li_2CO_3 on the pristine material, but also found that these compounds are no longer visible upon cycling.[119] Together, these findings are in agreement with reports that link the decomposition of native Li_2CO_3 to the onset of CO_2 evolution in the first cycle for layered transition metal oxides and imply that chemical or electrochemical methods may be used to remove them prior to battery operation.

Our group has used XPEEM to study the CEI that forms on NMC811 after 50 cycles in 1 M $LiPF_6$ in EC/DMC between 3.0 and 4.6 V vs Li/Li^+.[55] Upon charging to high voltage, residual Li_2CO_3 on the NMC811 surface reacts with HF in the electrolyte to form LiF, H_2O, and CO_2. LiF is left behind and remains selectively bound to the NMC811 particles only (where it can impact cell impedance) rather than the conductive carbon, as visualized in XPEEM (Figure 4B).[55] This mechanism agrees well with the onset of CO_2 evolution from Li_2CO_3 decomposition at earlier potentials (∼3.8 V[7,65]) and the dehydrogenation of EC that generates protons to form HF at the same voltage, the latter of which we detected with in situ solution NMR spectroscopy.[26,54,68] Note that a similar process likely also occurs on the surface of other Ni- and Li-rich layered materials that also can contain residual Li_2CO_3 on the surface, indicating that all of these structures suffer from having resistive LiF directly appended to the particle.

In contrast to the layered oxides, we find that the CEI on high-voltage spinel cathodes contains large quantities of MnF_2, rather than LiF, and that the metal fluorides are not localized to the active material surface (Figure 4C).[68] Upon cycling LNMO in the same electrolyte (1 M $LiPF_6$ in EC/DMC), MnF_2 ends up on the entire composite on both the active particles and the carbon additives in the film (Figure 4C). In addition, MnF_2 was found to decrease the electronic conductivity of the film by 3-fold compared to LiF. These results indicate that the CEI formed in LNMO-containing batteries with standard carbonate electrolytes has the combined effect of hindering Li transport to/from the active particles as well as decreasing the effectiveness of the conductive carbon. The distribution and physical behavior of LiF and other transition metal fluorides on cathode surfaces reinforces the need to be able to (i) identify each type of metal fluoride with high specificity, (ii) establish ways to measure their properties, and (iii) visualize their placement in the CEI.

The ability to probe the chemical composition of the CEI using sXAS with a lateral resolution of 70−180 nm makes XPEEM a useful tool to address items i and iii; when used in combination with a depth-resolved imaging technique (e.g., TOF-SIMS), we can create a 3D image of the CEI to evaluate prospective cathode materials, coatings, binders, and electrolyte formulations. For XPEEM measurements, the samples must be as flat as possible, so precise steps must be taken to minimize the surface roughness of the composite electrode prior to cycling. Typically, samples are isostatically pressed to approximately 2 tons before cell fabrication to obtain adequate lateral resolution. SEM imaging indicates that this procedure does not cause particle damage,[121] so this is not thought to impact the analytical results as this treatment may be similar to calendaring. Like other UHV methods, XPEEM requires sample washing and data collection under an X-ray beam. Beam damage can alter sensitive organic species, but collecting C K-edge spectra prior to higher energy edges can minimize this effect.[121] Unfortunately, XPEEM is a synchrotron-based technique, making it less accessible than other laboratory-based techniques.

3.4. Insights into the CEI Gained from Laterally Resolved Techniques. The collective studies on the CEI distribution on composite films show that where electrolyte decomposition products deposit on the electrode depends on the type of cathode material (for $LiPF_6$ salt in carbonate electrolyte) and that the distribution may impact the performance in different ways. For Ni-rich materials, Li_2CO_3, LiF, and carboxy-type structures attach directly on the active particle, while oligomers and vinyl species deposit all over the composite film possibly due to dissolution during cycling.[55,100] Similar findings have been reported for Li-rich materials, where metal fluorides concentrate on the particle itself and polymeric species spread out over the entire composite (covering both the carbon additives and the active particles), though comparative studies on each class of Li-rich materials are needed (e.g., Li_2MnO_3 vs Li-rich NMC).[100,119] The main difference that has been observed between the two layered cathodes (Ni vs Li rich) is the identity of solvent-derived CEI species, where the CEI on the Li-rich cathode contains polymeric structures while the Ni-rich cathode contains oligomers, vinyl, and carboxy species.[55,93,100] In relating the CEI to battery degradation, one of the more challenging

https://doi.org/10.1021/acsenergylett.3c01529
ACS Energy Lett. 2023, 8, 4572−4596

aspects is understanding how this seemingly simple change in composition may impact performance degradation. Both Ni- and Li-rich layered structures undergo a crystallographic reconstruction at the particle surface that often coincides with secondary particle cracking and impedance rise. Yet, without a quantitative, head-to-head comparison of these degradation modes together with an in-depth evaluation of the CEI (which is a large undertaking), we do not know how a more polymeric CEI might change the performance. For LNMO, transition metal fluorides (e.g., MnF_2, NiF_2) collect on active particles, but these species and other less soluble compounds, like Li_2CO_3 and LiF, decompose upon charge (due to locally high quantities of HF at the particle surface) and then reform during discharge where they can deposit on either the carbon or the active particle.[68,69,72,100] These findings are also relevant to the layered materials as their surface layer transitions to a spinel- or rocksalt-type structure (e.g., examining the CEI on the emerging class of disordered rocksalt cathodes may provide additional insight into how the CEI evolves).

Initial TOF-SIMS maps on LFP cathodes cycled in $LiPF_6$-containing carbonate electrolyte are consistent with a heterogeneous distribution of decomposition products on the LFP surface, though LFP is generally understudied compared to other materials.[103] This initial work conducted on LFP calls into question the role of LiF in CEI functionality, where it was detrimental to the rate capability. The impact of LiF on Li^+ and electron transport pathways may simply be more noticeable in LFP, where there are less solvent decomposition products to compensate. The instability of metal fluorides at high potential (which impacts the ionic and electronic conductivity of all cathode films) indicates that these species can be removed through high voltage pulsing. Another important point is that the exact location of LiF (and other fluorinated compounds) in the CEI likely depends on the formation pathway. For NMC composites that contain active materials with residual Li_2CO_3 on the surface, this can be directly converted to LiF that remains particle bound during cycling. Conversely, if LiF is formed in solution (e.g., from $LiPF_6$ dissociation) it does not necessarily precipitate out onto the active particle. At present, it is still unclear how interactions between carbon additives and liquid electrolytes impact the arrangement of the CEI, although their presence is correlated with increased quantities of C_2F^- and C_3OF^- species with $LiPF_6$ salt.[22]

Future work on electrolyte formulations with different anodic stability and alternative breakdown products will provide deeper insight into reactivity at the cathode/electrolyte interface, and approaches will likely differ based on cathode structure as well as type of carbon additive.

To date, a vast majority of the work has only been conducted in the presence of $LiPF_6$ and conventional carbonate electrolyte solvent, which is reported to form an uneven CEI layer.[24,55] While we can gather from TEM and TOF-SIMS that a "good" CEI is thin and conformal (correlating with high capacity retention and thermal stability for all cathode types), we still do not have an understanding of how to arrange certain electrolyte decomposition products to improve the battery performance. Future work on electrolyte formulations with different anodic stability and alternative breakdown products will provide deeper insight into reactivity at the cathode/electrolyte interface, and approaches will likely differ based on cathode structure as well as type of carbon additive (see Conclusions and Outlook).

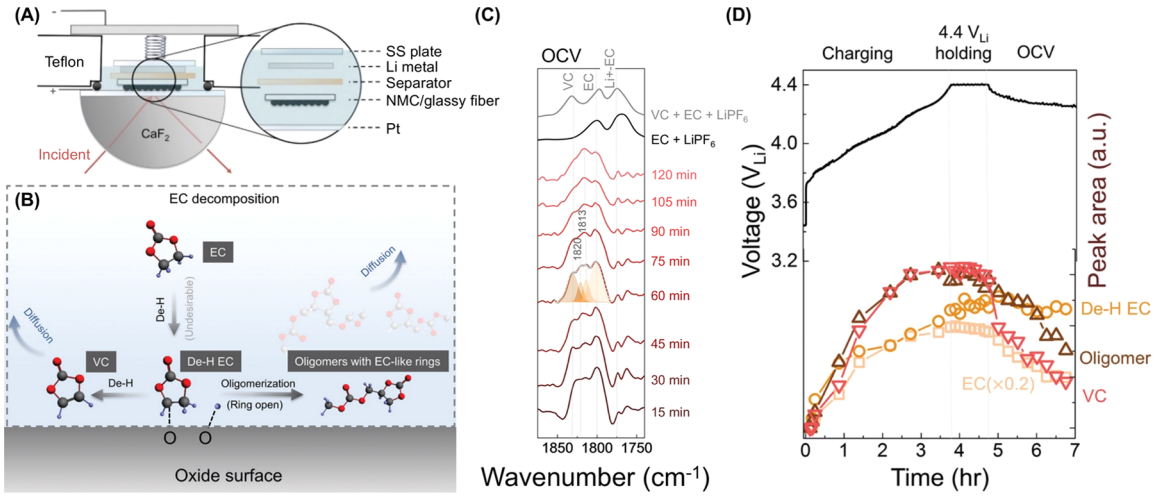

Figure 5. (A) Schematic of the in situ FTIR cell used with a composite cathode that has been drop cast onto a glassy fiber separator. (B) Proposed mechanism of electrolyte decomposition on NMC811 where EC is dehydrogenated at the surface to form VC or surface protons that further degrade the electrolyte. (C) In situ FTIR spectra collected at the surface of NMC811 during an open-circuit voltage (OCV) hold after charging to 4.4 V in 1.5 M $LiPF_6$ in EC. Deconvoluted peak areas plotted for the different species versus time show that EC decomposition products grow during charge. (D) Voltage profile (black) of NMC811 upon charging to 4.4 V, holding for 1 h, and resting at OCV. During the voltage hold, oligomers and VC diffuse away from the surface while dehydrogenated EC stays bound to the surface. Reproduced with permission from ref 26 under the CC-BY 3.0 license. Copyright 2020 The Royal Society of Chemistry.

https://doi.org/10.1021/acsenergylett.3c01529
ACS Energy Lett. 2023, 8, 4572−4596

4. TRACKING DECOMPOSITION AT THE CATHODE/ELECTROLYTE INTERFACE IN REAL TIME

While post-mortem characterization techniques are critical for characterizing the CEI on emerging cathode materials and electrolyte chemistries, these methods risk disruption of the sample through several modes, either by sample preparation (e.g., reaction of metastable CEI species due to consumption, sample rinsing, or other contamination) or during measurement (e.g., electron/X-ray beam exposure, UHV conditions, ion sputtering). As a result, it can be difficult or impossible to detect sensitive organic species and transient intermediates with ex situ methods, motivating the need for CEI characterization during battery operation. Additionally, it is challenging to quantify these species with ex situ techniques (e.g., comparing the absolute amount of CEI formed at charge vs discharge). In situ and operando analysis of the CEI circumvent these challenges and are particularly useful for revealing electrolyte oxidation pathways that lead to CEI formation. In this section, we highlight recent advances in in situ and operando methodologies that have elucidated cathode-driven degradation mechanisms previously inaccessible with ex situ approaches.

4.1. In Situ Fourier Transform Infrared (FTIR) and Raman Spectroscopies. Fourier transform infrared (FTIR) spectroscopy takes advantage of how chemical bonds respond to infrared light. Molecular bonds in a sample selectively absorb infrared radiation at specific wavelengths, leading to excitation of vibrational modes (e.g., stretching, bending). Raman spectroscopy also detects molecular vibrations through inelastic photon scattering upon irradiation with a laser at a particular wavelength. The resulting spectra are typically shown as a plot of transmittance (in wavenumber (cm^{-1})) versus intensity for FTIR or Raman shift (in cm^{-1}) versus intensity for Raman spectroscopy. Both techniques use similar setups for in situ battery studies with cells that allow light to penetrate the sample and interact with the interface of interest (Figure 5A).

In situ FTIR spectroscopy was one of the first CEI characterization tools used to detect electrolyte decomposition at the cathode in real time using molecular vibrations.[26,80] Initial in situ FTIR techniques developed for LFP and LCO informed our early understanding of CEI composition in standard carbonate electrolytes.[50,122−125] In 2005, Kanamura and co-workers found that when LCO is charged in 1 M $LiClO_4$ in EC/EMC, electrolyte oxidation begins at 3.8 V, forming carboxy-containing structures that may deposit on the surface or dissolve into the electrolyte.[125] They later used the same technique to analyze the electrochemical oxidation of 1 M $LiPF_6$ in EC/DEC with a LFP thin film cathode and found that no decomposition species were found during repeated charge/discharge processes in the potential range of 2.9−4.3 V, indicating that LFP does not undergo significant CEI formation in contrast to LCO. However, taking LFP up to 4.5 V resulted in electrochemical oxidation of the electrolyte, forming CO_2, Li carboxylates (RCO_2Li), Li alkyl carbonates ($ROCO_2Li$), and Li_2CO_3. This work emphasizes that LFP by itself is less reactive than LCO (the authors examined thin films without any carbon),[50,122,126] where they ultimately proposed that LFP could be used as a coating material for more energy-dense cathodes. In later work, Markevich and co-workers designed an in situ FTIR setup that tracked the formation of gaseous products upon cycling NCA composites in an ionic liquid electrolyte (0.5 LiTFSI in *N*-butyl-*N*-methylpyrrolidinium bis(trifluoromethanesulfonyl)amide), which is stable up to 5.5 V vs Li/Li^+.[127] The authors detected significant oxygen evolution from the cathode when cycled above 4.7 V, indicating that oxygen is released from layered oxide cathodes at high voltage, in agreement with online electrochemical mass spectrometry (OEMS), which can be difficult to perform in viscous ionic liquids.

Building on this work, Shao-Horn and co-workers designed a modified in situ FTIR setup (employing a composite cathode film rather than a thin film electrode) to compare electrolyte oxidation reactions that occur on a series of layered NMC-type cathodes as a function of Ni content (NMC111, NMC622, and NMC811, Figure 5).[26] For high Ni-content cathodes cycled in 1 M $LiPF_6$ in 3:7 EC/EMC, dehydrogenated EC molecules attach to the active particle surface upon charging to 3.8 V vs Li/Li^+, much lower than expected based on stability tests against Pt (EC is stable up to 4.8 V). After dehydrogenation, two further pathways are possible: dehydrogenated oligomers can detach from the particle surface or EC can be oxidized to vinylene carbonate (VC) in a two-electron process, which will also diffuse away from the surface. The dehydrogenation reaction was correlated with increased cell impedance that could be mitigated by switching from NMC811 to NMC111, coating the NMC811 with Al_2O_3, or using more concentrated electrolyte formulations (e.g., 3.1 M $LiPF_6$ in EC/EMC). These results suggest that the cell performance can be controlled by altering the electrolyte stability (by changing the solvation structure[128]) and/or the particle surface reactivity (possibly by tuning the nucleophilicity of surface oxygen, since surface reactivity decreases as NMC811 > NMC622 > NMC111[56]). This work provides important insight into a reaction pathway that produces VC at the cathode—a small molecule that is easily reduced to passivate the anode and therefore may be difficult to detect ex situ. However, this study raises an interesting question about why VC can impart beneficial properties at the anode (likely through the formation of poly(VC)) but is seemingly counterproductive when produced at the cathode.

Zhang and co-workers also used operando FTIR spectroscopy to examine the impact of adding 0.5% tris(trimethylsilyl)-borate (TMSB) to 1 M $LiPF_6$ in EC/EMC (1:2 v/v) when paired with the Li-rich cathode, $Li_{1.2}Ni_{0.2}Mn_{0.6}O_2$.[129] Operando FTIR spectroscopy showed that the TMSB-containing cell did not form significant quantities of vinyl species (C═C) upon charging to 4.8 V compared to the control electrolyte without TMSB. Upon discharge to 2.0 V, the CEI signal for the cell without TMSB grew significantly while the CEI signal for the TMSB-containing cell did not change, indicating that the additive allows stable surface passivation. The authors proposed that the electron-deficient boron atom in the additive weakens the solvation of $LiPF_6$ by EC by forming $[TMSB-PF_6]^-$ and $[TMSB-F]^-$ polyanion groups, resulting in reduced EC decomposition at the interface and formation of a thin CEI layer (~10 nm thick compared to ~50 nm thick after 250 cycles between 2.0 and 4.8 V). The fact that the intensity of the CEI signal varies upon lithiation/delithiation without the additive present indicates that decomposition products generated at the anode transfer to the cathode during discharge and vice versa, consistent with a lack of passivation and continuous electrolyte consumption. This observation also suggests that preventing the decomposition of EC into vinyl

https://doi.org/10.1021/acsenergylett.3c01529
ACS Energy Lett. 2023, 8, 4572−4596

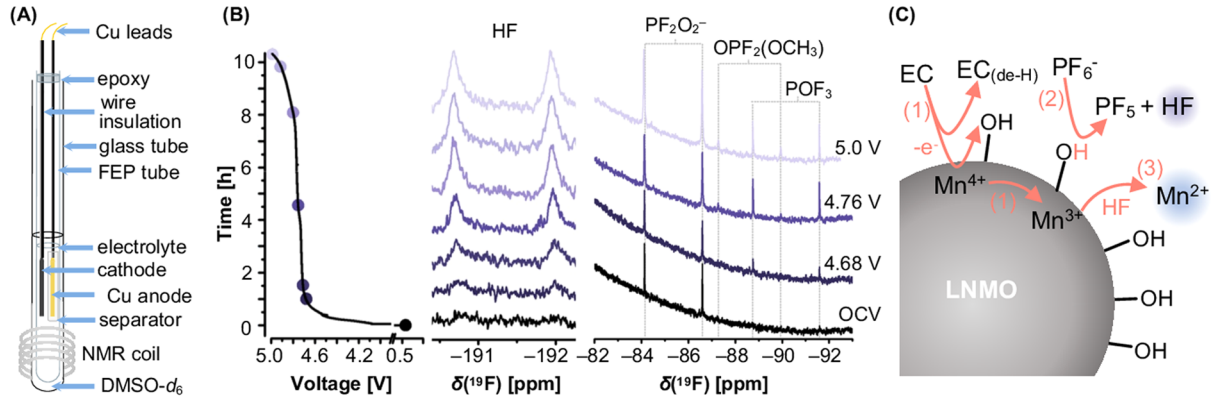

Figure 6. (A) Operando solution NMR cell containing a composite cathode vs a Cu current collector. (B) Select operando ^{19}F solution NMR spectra showing an increase in HF production and other $LiPF_6$ decomposition species upon delithiation of LNMO. (C) Proposed acid−base reaction between PF_6^- and surface-bound protons left behind from EC decomposition and resulting transition metal dissolution. Adapted with permission from ref 68. Copyright 2022 American Chemical Society.

species at the cathode is key to enhancing the performance of Ni-rich transition metal oxides.

In addition to FTIR spectroscopy, Raman spectroscopy has also been used to study the CEI during battery operation. Since the Raman response from the surface of bulk cathode materials is not sensitive enough for chemical characterization of the CEI,[130−132] Liu and co-workers introduced plasmonic nanoparticles to the cathode to obtain surface-enhanced Raman spectroscopy (SERS)[131−134] measurements while cycling NMC111 between 3.0 and 4.5 V in 1 M $LiPF_6$ in EC/DMC.[133] During the experiment, new vibrational modes appeared that were assigned to organic CEI species containing ether and ester functional groups that arise from electrolyte decomposition. After quantifying the amount of CEI present on the cathode at the top of charge and discharge, they found that low-Ni-content cathodes also exhibited evidence of dynamic CEI decomposition and/or anode−cathode crosstalk, especially regarding the lability of organic compounds in the CEI formed in conventional carbonate electrolytes.[73,74,93]

Taken together, these studies demonstrate that in situ vibrational spectroscopy provides a powerful toolset to study complex electrolyte decomposition reactions and CEI formation with excellent time resolution where spectra can be obtained every few minutes.[129] FTIR and Raman spectroscopies are accessible, nondestructive, and sensitive to organic molecules in the solution and the solid state. Although initial studies mostly used model thin film cathodes that are difficult to prepare, these techniques can also be translated to technologically relevant composite cathode films. In SERS, it is possible that the metallic nanoparticles interact with species in the CEI.[134,135] To address this potential caveat, researchers have implemented shell-isolated nanoparticle-enhanced Raman spectroscopy (SHINERS) to study the CEI, which is a variation of SERS that utilizes nanoparticles that are coated with an inert shell (such as SiO_2) to prevent interaction between the nanoparticles and the CEI.[132,134,136,137] For both FTIR and Raman spectroscopies, some signals may overlap due to a variety of bending and stretching modes which can complicate chemical assignments and may require comparison to computational models or other methods.[26,132,133]

4.2. In Situ/Operando Solution Nuclear Magnetic Resonance (NMR) Spectroscopy. Unlike FTIR or Raman spectroscopy, operando solution NMR spectroscopy cannot directly examine the cathode surface. Therefore, in situ/operando NMR spectroscopy is typically used to probe cathode reactivity in the solution state where the user can observe products from electrolyte oxidation reactions. In the solution state, NMR lines are more narrow due to fast molecular tumbling of small molecules, and therefore, the spectra provide better chemical resolution than in the solid state. Sample preparation for ex situ solution NMR spectroscopy often compromises reactive species formed during cycling by using deuterated solvents, glass NMR tubes, or simply opening the cell (e.g., HF is a volatile compound). Additionally, some electrolyte decomposition species, like VC, can be directly reduced at the anode, making ex situ detection challenging.[54]

In 2017, Nowak and co-workers developed an in situ NMR cell to study the liquid electrolyte inside of a two-electrode battery cell using high-resolution solution NMR spectroscopy.[138] In this setup, the authors used a cathode (NMC811)-coated Al rod surrounded by electrolyte/separator and a Li or graphite anode submerged in an inner, polymeric NMR tube that was placed inside of an outer glass NMR tube. A ^{19}F NMR spectrum was acquired from the NMC/Li in situ cell containing 1 M $LiPF_6$ in EC/DMC after holding at 4.3 and 4.6 V sequentially for 2 weeks and then at 4.9 V for 1 week at 60 °C. ^{19}F solution NMR spectroscopy detected the formation of FEC and fluoromethyl methyl carbonate (FMMC). These products were also observed in a room-temperature cell, though not until the voltage was ramped to 5.2 V, indicating that these species only form under extreme conditions. ^{1}H NMR spectroscopy of a NMC/graphite cell charged to 4.3 V at room temperature showed the formation of dimethyl 2,5-dioxahexanedioate (DMDOHD), which forms via reduction of the solvent at the anode.[139,140]

In 2022, we reported a modified in situ/operando cell design (Figure 6A) for high-resolution solution NMR and electron paramagnetic resonance (EPR) that uses cathodes cast onto standard Al foils and used it to study degradation in both NMC811 and LNMO batteries. In cells containing NMC811, we observed the formation of VC after cycling to 4.6 V in 1 M $LiPF_6$ in EC/DMC,[55] likely due to the dehydrogenation of EC, similar to the VC species detected by Shao-Horn and co-workers with in situ FTIR spectroscopy.[26] In addition, we also observed ^{1}H resonances appended to other unsaturated carbons (e.g., RC═CR′ groups), possibly due to formation of vinyl radicals that arise during electrolyte oxidation,[67,141]

https://doi.org/10.1021/acsenergylett.3c01529
ACS Energy Lett. 2023, 8, 4572−4596

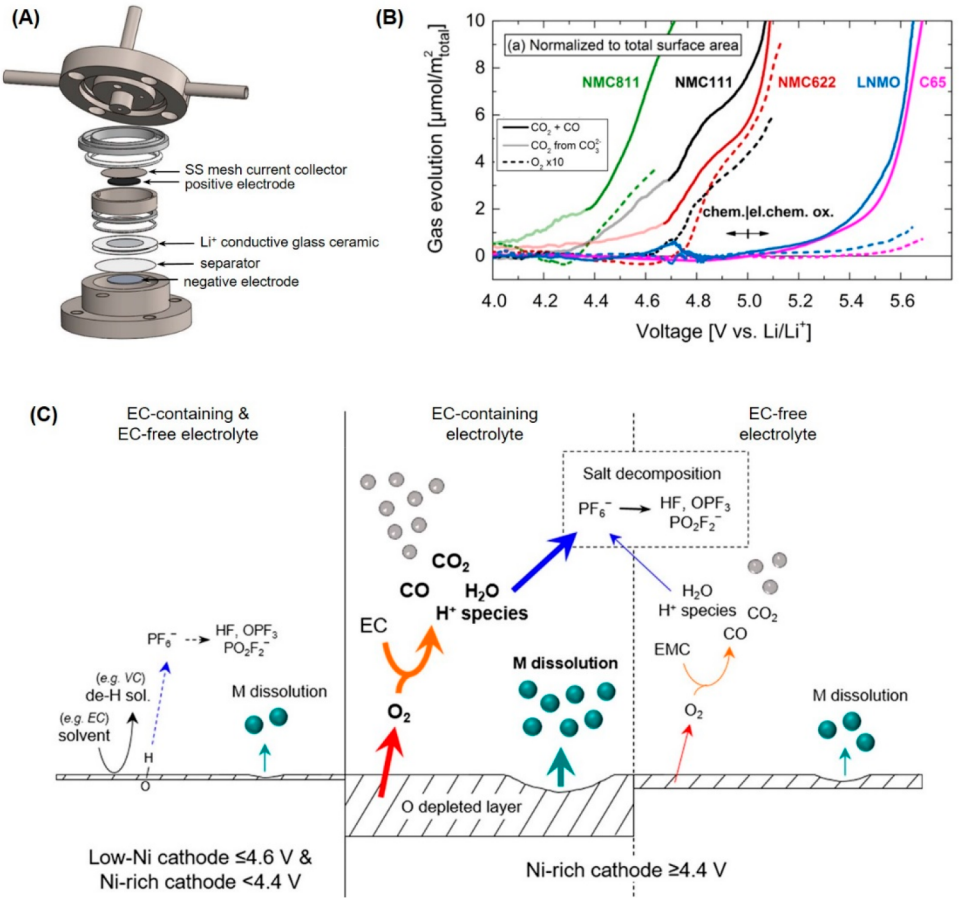

Figure 7. (A) Two-compartment OEMS cell that allows the separation of gases generated at the cathode and anode. Adapted with permission from ref 60. Copyright 2015 IOP Publishing. (B) Gas evolution detected via OEMS during a linear sweep to high voltage (>5 V) for different active materials (NMC811, NMC111, NMC622, LNMO) and conductive carbon (C65). Reprinted with permission from ref 61. Copyright 2017 American Chemical Society. (C) Proposed electrochemical and chemical oxidation mechanisms of EC and EMC determined from OEMS measurements and associated PF_6^- decomposition and transition metal dissolution. Reprinted with permission from ref 151. Copyright 2022 American Chemical Society.

signifying that a multitude of C═C components are associated with the performance decline in Ni-rich cathodes at high voltage. Additional work is needed to better understand the precise structure of these unsaturated carbons, the reactions that create them, and their functional effect on the CEI (e.g., it is unknown if they deposit on the cathode surface).

A subsequent study from our group examined the decomposition of 1 M $LiPF_6$ in EC/DMC during charging of LNMO using operando ^{19}F NMR spectroscopy (Figure 6) and correlated this with transition metal dissolution (observed via operando EPR).[68] Upon charging to 4.68 V vs Li/Li^+, we saw the formation of HF, $PO_2F_2^-$, $OPF_2(OCH_3)$, POF_3, and Mn^{2+}, all of which increase in concentration during delithiation to 5.0 V and indicate that there is a strong correlation between HF formation and transition metal dissolution. The ability to detect $LiPF_6$ decomposition products within the first hour of charging indicates that PF_6^- decomposition likely occurs by a mechanism that is distinct from $LiPF_6$ hydrolysis,[68] since hydrolysis in organic electrolytes occurs on the time scale of hours to days.[142,143] Instead, these findings support that $LiPF_6$ decomposition is accelerated by solvent oxidation reactions that protonate the transition metal oxide surface and generate dissolved protic species (e.g., solvent dehydrogenation).[25,29,57,67,77,144] Evidence of $LiPF_6$ decomposition at ~4.7 V in NMR spectroscopy is consistent with OEMS measurements on LNMO/Li cells where CO_2 evolution from EC oxidation starts around 4.76 V, suggesting that solvent oxidation and salt decomposition processes are coupled.[29] Terminal hydroxyl groups might be more acidic than the protons attached to water, which could lower the activation barrier for $LiPF_6$ decomposition (see the Insights into the CEI Gained from In Situ/Operando Techniques section for further discussion). This difference in kinetics that occurs in the presence of LNMO particles provides important mechanistic insight and could only be observed through operando measurements. Direct observation of the protic species generated during battery operation as well as quantitative values for the energy barrier for $LiPF_6$ decomposition (e.g., through variable-temperature experiments) may provide further clarity on how to mitigate transition metal dissolution.

In the aforementioned studies, our cell design contains planar electrodes with a large electrolyte volume (400 μL) that helps increase the signal-to-noise resolution for minor quantities of decomposition products.[27,145,146] However, this setup does not apply pressure to the system, leading to a limited lifetime of approximately 10 cycles. In contrast, the rolled cell design presented by Nowak and co-workers showed high capacity retention of 84% after 100 cycles, which we believe may be due to higher pressure in the electrode stack in this configuration. As a result, our planar electrode setup may

https://doi.org/10.1021/acsenergylett.3c01529
ACS Energy Lett. 2023, 8, 4572−4596

be more appropriate for detecting early-stage decomposition processes, whereas the rolled electrode configuration may be preferred to understand degradation over extended cycling.

Solution NMR spectroscopy is one of the few methods that can directly detect certain products, like HF (while simultaneously monitoring other species) during battery operation, which is critical to understanding how electrolyte decomposition drives transition metal leaching. However, there are a few factors that the user should be aware of. First, large amounts of transition metal dissolution, particularly dissolved Mn^{2+}, can broaden NMR signals, making it difficult to detect electrolyte decomposition products.[147] Second, the presence of HF in $LiPF_6$-based solutions requires that the cell be placed into a chemically resistant NMR tube as mentioned above. This setup conveniently allows the user to submerge the plastic in situ cell into a conventional NMR tube containing a deuterated solvent for locking and shimming to achieve high-resolution liquid NMR spectra.

4.3. Online Electrochemical Mass Spectrometry. Online electrochemical mass spectrometry (OEMS) and differential electrochemical mass spectrometry (DEMS) are operando techniques have been used extensively to detect the gases that are evolved during electrochemical cycling of a wide range of battery materials. OEMS measures the sum of all evolved gases versus time during electrochemical measurements, while DEMS directly measures the time derivative of this (yielding the gas evolution rates).[148] In an OEMS or DEMS experiment that analyzes anodic oxidation, gases released from a Swagelok-style cell are collected in the head space on the cathode side of the battery (Figure 7A) where an inert gas stream (typically Ar) passes them to a mass spectrometer for analysis based on their m/z ratio.[7,54,60] These gases are often the byproducts of CEI formation or species that lead to CEI growth, allowing the user to infer information about the reactions that occur at the cathode/electrolyte interface.

The anodic stability of the electrolyte can be monitored with LSV coupled with gas evolution detected with OEMS, which is essential for decoupling gases originating from cathode degradation. For example, Gasteiger and co-workers investigated the electrochemical decomposition of 1 M $LiPF_6$ in EC:EMC (3:7 w/w) using a Super P C65/PVDF working electrode to study the anodic stability of minor species in battery-grade electrolyte.[58] Upon intentional addition of impurities such as ethylene glycol and ethanol to the electrolyte, the authors observed an increase in current at 3.5 V that coincides with the evolution of PF_5/POF_3. At this potential, no CO_2 is produced, and the authors ascribe this observation to the electrochemical oxidization of the impurities that produces protic species (H^+) that can react with PF_6^- salt to form HF and PF_5. Once the voltage exceeds 4.5 V, CO_2 release increases exponentially, signifying the onset of electrochemical oxidation of the solvent, which produces additional H^+ that feeds into the same reaction pathway.

When Li_2CO_3 is mixed into the composite electrode, CO_2 evolution occurs at the same voltage (~3.5 V vs Li/Li^+) as PF_5/PO_3 gassing, indicating that salt decomposition and native carbonate degradation are strongly coupled. No O_2 evolution was noted. These observations are consistent with OEMS and DEMS results from other groups that discovered that Li_2CO_3 decomposition starts between 3.7 and 4.0 V and continues at higher voltages until it is consumed, largely contributing to CO_2 generated in the first cycle (~33−50% of CO_2 generation[64,149,150]).[6,7,64] The fact that none of these studies observe O_2 evolution in the voltage range attributed to Li_2CO_3 decomposition indicates that Li_2CO_3 is not electrochemically oxidized ($Li_2CO_3 \rightarrow 2Li^+ + 2e^- + 1/2O_2 + CO_2$) but rather chemically decomposes to form insoluble LiF, which is an important CEI component that likely remains bound to the active particle surface ($Li_2CO_3 + 2HF \rightarrow 2LiF + H_2O + CO_2$).[65] Further, this work implies that the synthesis and handling of cathodes directly impacts the amount of Li_2CO_3 on the particle surface and thus the quantity of LiF in the CEI since it is catalytically converted to LiF by HF. On the other hand, the source of protic species is more nebulous—the intentional addition of ethylene glycol and ethanol suggests that minor impurities can generate H^+, but it is also possible that small quantities of water or other electrolyte solvent decomposition reactions that do not produce gases may also serve as proton sources.

With an understanding of how trace components impact CEI formation, we next examine how oxygen release from the active particles contributes to CEI growth.[27,151] Gasteiger and co-workers have conducted multiple studies comparing gas release from NMC111, NMC622, NMC811, and LNMO.[6,61,148] Jung et al. showed that O_2 evolution upon delithiation is accompanied by a steep increase in CO_2 and CO evolution in NMC111, NMC622, and NMC811 cells due to the onset of chemical oxidation of the electrolyte (Figure 7B),[61] likely due to the reactivity of terminal oxygen atoms on the surface of active particles. In the NMC series, when oxygen is removed from the lattice, the particle surface undergoes crystallographic reconstruction to a rocksalt phase that coincides with chemical oxidation of the electrolyte from attack by singlet oxygen. In the layered oxides, EC can react with singlet oxygen to generate CO_2, CO, and H_2O at deep states of delithiation;[6,61] H_2O can of course participate in the hydrolysis of $LiPF_6$ to form LiF and/or transition metal fluorides from HF etching of the particle surface that deposits in the CEI. In more complex electrolyte formulations, singlet oxygen can also attack linear carbonates and electrolyte additives (e.g., FEC, VC) to form polycarbonates or carboxylic acids that deposit on the cathode surface.[27,141,152,153] However, these molecules appear to be more resistant to $^1O_2$ attack, and the role of these minor reaction byproducts in surface stability is not well established (vide infra).

Recent work by Grey and co-workers supports that the low onset voltage for O_2 loss in Ni-rich NMCs is tied to interactions between the electrolyte and the active particle surface, with EC being particularly problematic in combination with NMC811.[151] When both low-Ni-content and high-Ni-content NMCs are cycled below 4.4 V, no O_2 evolution is observed, regardless of whether or not EC is present in the electrolyte (Figure 7C). In agreement with prior literature reports,[25,26,68] the authors propose that EC undergoes a dehydrogenation reaction at low potential, where deprotonation leads to HF formation and Mn dissolution. At this point, surface reconstruction is limited to the first few atomic layers. Upon charging Ni-rich NMC811 past 4.4 V, OEMS measurements detect substantial O_2 release from the cathode in EC-containing electrolytes that is concomitant with CO and CO_2 generation and increased thickness of the surface reconstruction layer visualized with HRTEM.[154] When cyclic EC is replaced with linear EMC, the total amount of O_2 loss is reduced along with other degradation processes that hinder battery performance (e.g., surface reconstruction, increased

https://doi.org/10.1021/acsenergylett.3c01529
ACS Energy Lett. 2023, 8, 4572−4596

resistance, transition metal dissolution, additional electrolyte decomposition).

Density functional theory (DFT) calculations suggest that singlet oxygen can react with EC to form peroxide and VC.[155] In turn, VC may then electrochemically oxidize to form a polymer coating on the surface of the NMC811 particle, although the onset voltage of the electrochemical oxidation of VC is still unclear. In combination with conductive carbon-based working electrodes, one report suggests that VC oxidation occurs at 4.7 V vs Li/Li^+ when at 0.5 wt %,[156] while another indicates that VC oxidation and CO_2 evolution starts at 4.3 V when it is the sole solvent.[141] This difference in onset voltage makes a major difference in terms of the chemical composition of the CEI given the operating voltage of common cathode materials. Under the same conditions, DFT predicts that linear carbonates are less susceptible to attack by singlet oxygen. Upon attack, small quantities of poorly passivating linear fragments, like alcohols and carboxylic acids, along with Li_2CO_3 are observed in the CEI. Either way, the difference in reactivity between the cyclic and the linear carbonates gives a positive correlation between O_2 evolution and the thickness of both the CEI and the surface reconstruction layer in electrolytes that contain cyclic molecules.[157] Additional work should be carried out to understand the mechanism by which VC seemingly prevents surface reconstruction. A more granular look at the impact of the layered transition metal oxide composition on O_2 evolution shows that the intrinsic stability limit (where O_2 release leads to chemical decomposition of the solvent) varies from 66% SOC for LCO, 65% SOC for NMC111, to 86% SOC for NMC851005[58] and that this process is worse for Li-rich layered materials due to activation of Li_2MnO_3[158] and the fact that the transition metal layer is less stable after Li removal.[7,144,158] As a result, we can expect that impedance buildup from crystallographic changes and organic matter in the CEI will be worse for high energy density cathodes.

Taken together, these data suggest that when pairing electrolytes with cathodes that release O_2, we must consider that not all carbonates exhibit the same stability toward singlet oxygen, where cyclic EC is especially vulnerable. Instead, electrolyte design strategies that functionalize the C2 or C3 position on EC (e.g., FEC[153]) to prevent stabilizing intermediates that result after oxygen attack may prevent CEI buildup in layered cathodes. Alternatively, modifying the particle surface to tune EC coordination with the layered host to mitigate the extent of oxygen evolution may also improve the battery performance. This thick, solvent-derived CEI observed with the layered structures is distinct from the spinels, which do not evolve O_2 at typical operating voltages. Therefore, we do not expect singlet oxygen to play a role in electrolyte breakdown and CEI formation for these materials but rather electrochemical oxidation. Protic species that facilitate PF_6^- salt decomposition and HF formation can enable transition metal leaching and degradation of the conductive carbon matrix at high voltage, ultimately hindering electronic conductivity and connectivity.

So far, we have primarily focused on using OEMS/DEMS to study the production of O_2, CO_2, and/or CO, but it can also be used to track the rate of decomposition of the electrolyte salt (e.g., $LiPF_6$). In particular, the operando nature of OEMS also provides insight into the kinetics of $LiPF_6$ decomposition in the presence of oxidized carbonate solvents.[67] Gasteiger and co-workers reported that protic species formed by carbonate oxidation lead to fast dissociation of $LiPF_6$ at room temperature by monitoring gas evolution at different temperatures (10−80 °C) for a solution of 1.5 M $LiPF_6$ in EC after the addition of 5000 ppm methane-sulfonic acid (in the absence of active electrodes/electrochemistry).[67] POF_3 is detected within the first hour of resting at 25 °C, plateauing at approximately 1000 ppm by 3 h. At higher temperatures, the kinetics of this reaction increase, where POF_3 reaches a maximum only 1 h into the following 3 h rest steps at 40, 60, and 80 °C. Another study by the same group used single- and two-compartment OEMS NMC/graphite cells containing 1 M $LiPF_6$ in EC/EMC (3:7 by weight) to demonstrate that these protic species are reduced to H_2 at the graphite anode, one of the main gases found in LIBs after long-term cycling.[159] The most H_2 gas is produced in cells with high upper cutoff voltages (4.6 V), where more electrolyte oxidation/protic species are produced at the cathode, highlighting the fact that deep delithiation poses serious safety concerns in $LiPF_6$-based batteries.

Although a majority of DEMS/OEMS reports have mostly focused on carbonate-based electrolytes, more recent work has applied this technique to study gas release in systems that use more specialized electrolyte formulations. For example, Manthiram and co-workers compared the gas evolution from an Ni-rich cathode ($LiNi_{0.94}Co_{0.06}O_2$) when cycled in localized high-concentration electrolyte (LHCE) (LiFSI:DME:TTE 1:1.2:3 by mole) versus standard carbonate electrolyte (LP57).[160] The 5× improvement in capacity retention after 200 cycles for the LHCE cells was associated with a 3× reduction in gas evolved from the cells charged to 4.3 V compared to the carbonate electrolyte. It is well known that the unique solvation structure found in LHCEs (e.g., contact-ion pairs) lowers the free energy of the electrolyte and improves the anodic stability. In addition, the major solvent, TTE (1,1,2,2-tetrafluoroethyl-2,2,3,3-tetrafluoropropyl ether), is mostly comprised of C−F bonds that are extremely difficult to cleave and resistant to attack. Similarly, LiFSI is less prone to HF formation compared to $LiPF_6$. By minimizing parasitic reactions at the cathode surface, we can also prevent surface reconstruction and particle cracking in Ni-rich cathodes—phenomena that are thought to be caused by the lithiation state of the bulk particle but may actually be linked to CEI formation.

Overall, this section demonstrates that OEMS/DEMS offer excellent chemical resolution to monitor the gases evolved during battery operation with a detection limit in the range of tens of ppm and a time resolution of ∼3 s.[161] A notable exception to this was reported by Solchenbach et al., who found that OEMS cannot distinguish PF_5/POF_3, and thus, their sum is detected during measurement.[67] One drawback to OEMS is that it may not detect dissolved gases in the electrolyte and that not all decomposition reactions generate gas (e.g., the dehydrogenation of EC into VC[54]). Gas evolution from the anode and cathode can be decoupled from one another by comparing data from single- versus two-compartment cells (where the anode and cathode are kept in separate chambers using a gas-impermeable but ion-permeable separator).[60] Further, the use of an LFP counter electrode or two-compartment cells is advised for evaluating CO_2 production originating from positive electrodes as CO_2 is actively consumed at the anode when using graphite or Li counter electrodes.[54,58,60,155] Several discrepancies in the literature with OEMS measurements also arise from carbonate

https://doi.org/10.1021/acsenergylett.3c01529
ACS Energy Lett. 2023, 8, 4572−4596

impurities or active material vs surface area in the working cell. Reference 61 provides a good example calculation for how to estimate the upper limit of CO_2 that can be evolved from residual Li_2CO_3.[61]

4.4. Insights into the CEI Gained from In Situ/Operando Techniques. Since most of the in situ studies performed to date have focused on the layered-type (NMC) and the spinel-type (LMO/LNMO) cathode materials cycled in 1 M $LiPF_6$ salts coupled with carbonate solvents, we will summarize the combined insight from this body of work in the context of both systems. Let us examine what generally occurs at the cathode side of the battery step-by-step during charging (delithiation) at room temperature. In both Ni-rich NMC cathodes (e.g., NMC811) and Mn-rich spinels, in situ FTIR and NMR spectroscopies indicate that with carbonate molecules, dehydrogenation occurs at low states of charge[26,29,54−56] (e.g., approximately 3.8−4.1 V for NMC, Figure 5A), likely in tandem with transition metal reduction[54,57] as shown in Scheme 1.

Scheme 1. Proposed Reaction Mechanism for the Coupled Dehydrogenation of EC (A) and Protonation of the Transition Metal Oxide Cathode Surface (B) That Occurs during Delithiation[a]

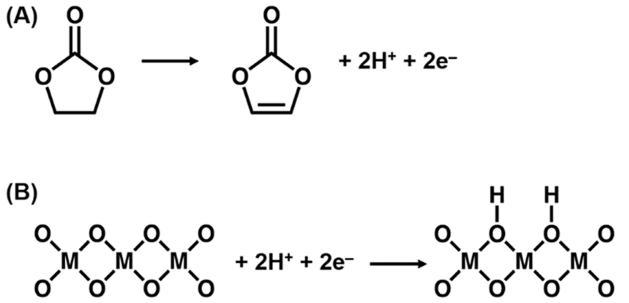

[a]Note that B also includes reduction of the transition metal centers.

Scheme 1 shows the protons from the dehydrogenation reaction of EC appended to the active material surface. Although the precise form of these protic species is not known (e.g., surface hydroxyl groups, H_2O_{oxide}, and/or H_2O_{2oxide}[25,54,68] have been proposed), they can all go on and participate in further side reactions. The dehydrogenation of EC is simply one example where solvent molecules will release protons; other cosolvents and impurities (e.g., linear carbonates, glycols, alcohols) can also undergo oxidation and generate H^+ at low voltage (<4.2 V). In nearly every scenario, the removal of protons from the solvent (to generate vinyl compounds in the CEI and catalytically active H^+) is correlated with surface reconstruction at the particle surface that manifests in the form of increased impedance and capacity fade.

Reactive H^+ species generated during solvent decomposition then lead to $LiPF_6$ decomposition.[67,162] Using operando NMR spectroscopy, we see that the rate of $LiPF_6$ decomposition in the presence of LNMO occurs much quicker than expected for a simple hydrolysis reaction (on the time scale of minutes vs days).[68,142] The faster kinetics observed in an actual battery is likely due to the presence of these protic species (e.g., surface hydroxyls) that are more acidic than water and therefore can catalyze the decomposition of $LiPF_6$ into HF (Figure 5B and Scheme 2). Given that similar solvent decomposition reactions

Scheme 2. Proposed Reaction Mechanisms in Which Protic Species on the Cathode Surface Catalyze the Decomposition of PF_6^- into HF and PF_5 (A), PF_5 Chemically Reacts with Water To Generate POF_3 and HF (B), and POF_3 Reacts with Water To Form Additional HF and HPO_2F_2 (C) in Nonaqueous Electrolyte

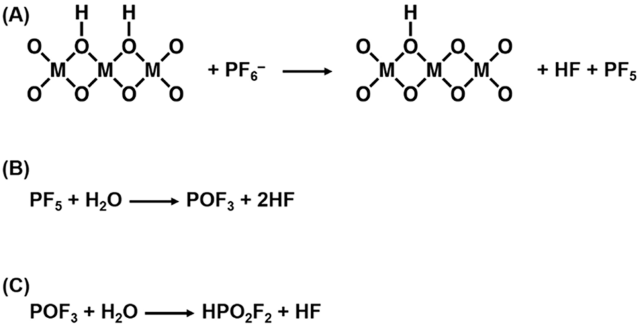

take place upon the initial delithiation of both spinel and layered materials, we expect both systems to follow similar pathways for the formation of HF.

In both surface/proton-catalyzed $LiPF_6$ decomposition as well as $LiPF_6$ hydrolysis, HF in the electrolyte can react with residual Li_2CO_3 on the cathode starting as low as 3.8 V, according to DEMS,[7] producing surface-bound LiF, H_2O, and CO_2 (Scheme 3). The LiF deposits on the particle surface and

Scheme 3. Proposed Reaction Mechanism for the Chemical Decomposition of Residual Surface Li_2CO_3 via HF into Particle-Bound LiF, H_2O, and CO_2

$$(Li_2CO_3)_{CEI} + 2HF \longrightarrow (2LiF)_{CEI} + H_2O + CO_2$$

likely impacts Li insertion/removal.[55] If HF in the electrolyte does not have Li_2CO_3 to react with, it will attack the active particle surface and dissolve transition metals (e.g., Ni, Mn, Fe, and Co depending on the composition); these processes can also happen concurrently. Differences in native CEI chemistry and moisture sensitivity between LMO-based structures and layered materials as well as Mn oxidation state at the particle surface (Mn^{3+} is susceptible to acid-driven disproportionation) may explain the different trends that have been observed for transition metal dissolution.[23,163] For example, if NMC-type structures have more Li_2CO_3 that can be used to "scavenge" HF and all of the Mn is in the 4+ oxidation state then they will not suffer from as much transition metal dissolution. This scavenging effect is similar to coatings, such as Al_2O_3,[72] and is supported by the fact that the CEI on spinel cathodes shows lower quantities of LiF compared to NMC811.[68,164] Recall that Figure 5C also shows little CO_2 evolution at low voltages for LNMO compared to NMC attributed to native Li_2CO_3.[61] We note that one major gap in characterization at present is the ability to distinguish between different oxidation states in dissolved transition metals in situ. This information would offer more clarity on the mechanisms that link metal leaching with performance degradation in different cathode structures.

Upon charging to higher voltage (>4.3 V), Gasteiger and co-workers used OEMS to show that the layered cathodes release singlet oxygen ($^1O_2$) that can oxidize EC, producing CO_2, CO, and water (Scheme 4).[58,61] Such reactions have been directly correlated with growth of a spinel/rocksalt reconstruction layer at the active particle surface.[64,154,165] Water can then hydrolyze

https://doi.org/10.1021/acsenergylett.3c01529
ACS Energy Lett. 2023, 8, 4572−4596

Scheme 4. Proposed Reaction Mechanism for the Chemical Oxidation of EC by Singlet Oxygen Evolved from Cathode Active Material at High States of Charge To Form CO_2, CO, and Water

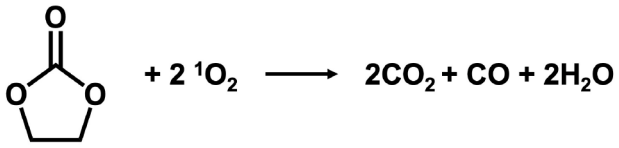

both the salt anions as well as the electrolyte solvent molecules,[27,54] exacerbating decomposition reactions that have already occurred at lower voltage. As expected, the activation of Li-rich materials in which oxygen escapes the lattice was also associated with increased $LiPF_6$ decomposition.[144] Note that at this point linear carbonates are also chemically oxidized by singlet oxygen, where OEMS indicates that the reaction with EMC produces ethanol, CO_2, CO, and water.[151] Likewise, in situ NMR spectroscopy clearly shows the formation of $OPF_2(OCH_3)$ from the reaction between DMC and POF_3 upon cycling spinel cathodes.[68] A wide variety of other electrolyte fragments and salt decomposition products are observed upon cycling above 4.3 V due to reaction with oxygen and other reactive byproducts that have not been described in depth here but may play a role in CEI stability at high potential.[25,27,54,93,100,166] Once the system exceeds 4.5 V, the solvent may also undergo electrochemical oxidation (in addition to chemical oxidation from reactive oxygen species), generating more protic species (ROH) that exacerbate $LiPF_6$ decomposition, HF formation, and transition metal dissolution.[6,58,67,144,148] These protons are reduced at the anode and released as H_2 gas, which leads to swelling in pouch cells and compromised safety when cycled >4.5 V.[159,167]

From this insight there are obvious routes forward to mitigate electrolyte decomposition in high-energy cathodes for LIBs, and we can project how these characterization methods may adapt to understand the resulting CEI. Both $LiPF_6$ and EC present major problems in combination with high-energy cathodes, and replacing these components with more stable salts and solvents is critical but presents their own set of challenges. For example, LiFSI salt is less susceptible to hydrolysis (but to the best of our knowledge other mechanisms of HF formation have not been rigorously examined) yet is corrosive and has safety concerns.[168,169] Most high-performing electrolytes include highly fluorinated components, including the salt and solvent. The fluorinated salt is often correlated with increased quantities of transition metal fluorides in the CEI that are poor ion/electron conductors that may dissipate at high voltage. Fluorinated solvents improve the oxidative stability of the electrolyte compared to conventional carbonate systems, where the byproducts (e.g., vinyl compounds) of both cyclic and linear carbonates fail to suppress side reactions. In contrast to completely changing electrolyte formulation, recent work suggests that high-potential holds (5.4 V vs Li/Li^+) can stabilize the organic CEI formed in EC/DMC and passivate the electrode surface,[152] offering another way to improve cycle life. Regardless of the strategy, pairing a given cathode with an optimized electrolyte that has high anodic stability will limit side reactions, ultimately making CEI formation pathways more challenging to track in situ. Improving the limit of detection for each operando methodology discussed in this section will become absolutely necessary; for example, using a cryoprobe for NMR measurements to minimize thermal noise and increase signal-to-noise resolution or using surface-enhanced vibrational spectroscopies may offer additional sensitivity.

Regardless of the strategy, pairing a given cathode with an optimized electrolyte that has high anodic stability will limit side reactions, ultimately making CEI formation pathways more challenging to track in situ. Improving the limit of detection for each operando methodology will become absolutely necessary.

In comparison to other commercially relevant materials, considerably less in situ work has been carried out to study the electrolyte decomposition processes that occur in LFP-containing batteries.[123,161] LFP is less reactive than the layered or spinel materials, so it presents characterization challenges because of its thin CEI. LFP has a lower operating voltage than NMC and therefore is not expected to suffer from the electrolyte oxidation and subsequent degradation that takes place during cycling. Despite this difference in reactivity, recent work suggests that NMC532 outperforms LFP in terms of capacity retention when the upper cutoff voltage of NMC532 is limited to 3.8 V.[105,170,171] Dahn and co-workers rationalized this behavior by indicating that reactions between the cathode and the electrolyte in this cycling regime (3.0−3.8 V) are beneficial for the graphite anode, while the absence of decomposition at the cathode in LFP cells (cycled 2.5−3.65 V) prevents the formation of a passivating anode SEI.[171] In this particular system, the authors use a carbonate solvent system (EC/DMC with 2% wt VC) and test both $LiPF_6$ and LiFSI salts at moderate concentration (1.5 M). At least in the $LiPF_6$ system, we expect that the cells just reach the onset for solvent dehydrogenation, HF formation, and Li_2CO_3 breakdown (Schemes 1−3) that will indeed impact the anode SEI through chemical crosstalk. The formation of electrolyte oxidation products likely does not occur in LFP cells due to its chemical stability with esters. Additional work still needs to be done to understand how LiFSI can influence the CEI in both systems.

We note that LFP may also not be completely immune from surface-driven decomposition reactions. Previous reports have shown that LFP is moisture sensitive and that if the material is not thoroughly dried, the surface will exhibit hydroxyl groups that can react with the electrolyte[105] through a route that may resemble that of high-voltage cathodes. Although LFP is generally considered a CEI-free material in standard $LiPF_6$-containing carbonate electrolytes,[33,172] closer examination of how handling conditions impacts battery performance may provide the insight needed to enable longer lasting batteries. The recent drive to adopt iron−phosphate-containing batteries due to their materials abundance has generated renewed interest in olivines with more energy density, such as $LiMn_xFe_{1-x}PO_4$ (LMFP) cathodes, for which the surface reactivities are even less understood.[173]

https://doi.org/10.1021/acsenergylett.3c01529
ACS Energy Lett. 2023, 8, 4572−4596

5. CONCLUSIONS AND OUTLOOK

The work outlined in this review displays major achievements in characterization that allow new insights into the composition, structure, arrangement, and formation mechanisms of the CEI for both conventional and emerging cathode materials. The combination of spatially and temporally resolved characterization techniques tends to agree that poor ion conductors like Li_2CO_3, LiF, and transition metal fluorides that coat the electrode surface impede Li-ion intercalation during electrochemical cycling despite the fact that these compounds are often correlated with enhanced battery performance. The concentration of inorganic compounds in the CEI that impart beneficial properties may depend on factors like the spatial distribution and particle size, pointing to the utility of depth and lateral resolution. Through the lens of these advanced characterization tools, there is increasing evidence that the organic solvent decomposition plays an active role in cathode degradation given that it is coupled to transition metal reduction at the particle surface, salt breakdown kinetics, crystallographic reconstruction, and secondary particle cracking. However, the organic CEI is the portion that we still know the least about, and learning more about the exact chemical makeup, arrangement, and formation mechanisms may elucidate new pathways to mitigate performance decline.

Overall, we look forward to the application of advanced characterization techniques to more sophisticated electrolyte formulations (e.g., with alternative salts, solvents, and additives), coatings, and electrochemical treatments that can minimize degradation at the cathode and anticipate a push to coupling spatially resolved methods with approaches that can monitor the CEI in situ. At present, a large barrier to in situ/operando characterization techniques is the need for custom-made cells that do not resemble practical batteries. We expect that future analytical techniques will focus on developing operando cells that are more representative of practical devices while retaining the same chemical, spatial, and/or temporal resolution. Ideally, we want to be able to simultaneously characterize electrolyte oxidation reactions as they occur and the eventual fate of those byproducts in the cell (do they deposit in the CEI or do they travel to the anode side of the battery), but it is very difficult to capture all of these things in practice. In moving toward this goal, one strategy may be to combine multiple techniques to, for example, monitor the spatial distribution of degradation products along with gas evolution and changes in CEI composition. We expect that innovative characterization tools will continue to offer critical information on cathode-driven degradation processes that help address lifetime and safety issues in LIBs and accelerate adoption of new technologies.

AUTHOR INFORMATION

Corresponding Author

Lauren E. Marbella − *Department of Chemical Engineering, Columbia University, New York, New York 10027, United States;* orcid.org/0000-0003-1639-3913; Email: lem2221@columbia.edu

Author

Julia C. Hestenes − *Program of Materials Science and Engineering, Department of Applied Physics and Applied Mathematics, Columbia University, New York, New York 10027, United States*

Complete contact information is available at: https://pubs.acs.org/10.1021/acsenergylett.3c01529

Notes

The authors declare no competing financial interest.

Biographies

Julia C. Hestenes is a Ph.D. candidate and NSF Graduate Research Fellow in the Materials Science & Engineering Program at Columbia University, where she is supervised by Lauren Marbella. Her thesis focuses on developing spatially and temporally resolved spectroscopies to study the CEI and electrolyte decomposition in LIBs.

Lauren E. Marbella is currently an Associate Professor of Chemical Engineering at Columbia University, where her group focuses on understanding the relationship between interfacial chemistry and performance in electrochemical energy storage systems with an emphasis on NMR characterization techniques.

ACKNOWLEDGMENTS

This work was supported by National Science Foundation CAREER Award (CBET-2045262). J.C.H. was supported by the National Science Foundation Graduate Research Fellowship Program (NSF GRFP No. 2021278071).

REFERENCES

(1) Frith, J. T.; Lacey, M. J.; Ulissi, U. A Non-Academic Perspective on the Future of Lithium-Based Batteries. *Nat. Commun.* **2023**, *14*, 420.

(2) Goodenough, J. B.; Kim, Y. Challenges for Rechargeable Li Batteries. *Chem. Mater.* **2010**, *22*, 587−603.

(3) Gourley, S. W. D.; Or, T.; Chen, Z. Breaking Free from Cobalt Reliance in Lithium-Ion Batteries. *iScience.* **2020**, *23*, 101505.

(4) Grey, C. P.; Hall, D. S. Prospects for Lithium-Ion Batteries and beyond—a 2030 Vision. *Nat. Commun.* **2020**, *11*, 6279.

(5) Fu, W.; Kim, D.; Wang, F.; Yushin, G. Stabilizing Cathodes and Interphases for Next-Generation Li-Ion Batteries. *J. Power Sources* **2023**, *561*, No. 232738.

(6) Jung, R.; Metzger, M.; Maglia, F.; Stinner, C.; Gasteiger, H. A. Oxygen Release and Its Effect on the Cycling Stability of LiNi x Mn y Co z O 2 (NMC) Cathode Materials for Li-Ion Batteries. *J. Electrochem. Soc.* **2017**, *164* (7), A1361−A1377.

(7) Renfrew, S. E.; McCloskey, B. D. Residual Lithium Carbonate Predominantly Accounts for First Cycle CO2 and CO Outgassing of Li-Stoichiometric and Li-Rich Layered Transition-Metal Oxides. *J. Am. Chem. Soc.* **2017**, *139* (49), 17853−17860.

(8) Kong, F.; Liang, C.; Wang, L.; Zheng, Y.; Perananthan, S.; Longo, R. C.; Ferraris, J. P.; Kim, M.; Cho, K. Kinetic Stability of Bulk LiNiO2 and Surface Degradation by Oxygen Evolution in LiNiO2-Based Cathode Materials. *Adv. Energy Mater.* **2019**, *9* (2), No. 1802586.

(9) Lin, F.; Markus, I. M.; Nordlund, D.; Weng, T. C.; Asta, M. D.; Xin, H. L.; Doeff, M. M. Surface Reconstruction and Chemical Evolution of Stoichiometric Layered Cathode Materials for Lithium-Ion Batteries. *Nat. Commun.* **2014**, *5*, 3529.

(10) Xu, C.; Märker, K.; Lee, J.; Mahadevegowda, A.; Reeves, P. J.; Day, S. J.; Groh, M. F.; Emge, S. P.; Ducati, C.; Layla Mehdi, B.; Tang, C. C.; Grey, C. P. Bulk Fatigue Induced by Surface Reconstruction in Layered Ni-Rich Cathodes for Li-Ion Batteries. *Nat. Mater.* **2021**, *20*, 84−92.

(11) Carroll, K. J.; Qian, D.; Fell, C.; Calvin, S.; Veith, G. M.; Chi, M.; Baggetto, L.; Meng, Y. S. Probing the Electrode/Electrolyte Interface in the Lithium Excess Layered Oxide Li1.2Ni0.2Mn0.6O2. *Phys. Chem. Chem. Phys.* **2013**, *15* (26), 11128−11138.

(12) Liu, T.; Dai, A.; Lu, J.; Yuan, Y.; Xiao, Y.; Yu, L.; Li, M.; Gim, J.; Ma, L.; Liu, J.; Zhan, C.; Li, L.; Zheng, J.; Ren, Y.; Wu, T.; Shahbazian-Yassar, R.; Wen, J.; Pan, F.; Amine, K. Correlation

between Manganese Dissolution and Dynamic Phase Stability in Spinel-Based Lithium-Ion Battery. *Nat. Commun.* **2019**, *10* (1), 4721.
(13) Lin, M.; Ben, L.; Sun, Y.; Wang, H.; Yang, Z.; Gu, L.; Yu, X.; Yang, X. Q.; Zhao, H.; Yu, R.; Armand, M.; Huang, X. Insight into the Atomic Structure of High-Voltage Spinel Lini0.5mn1.5o4 Cathode Material in the First Cycle. *Chem. Mater.* **2015**, *27* (1), 292−303.
(14) Aurbach, D.; Markovsky, B.; Talyossef, Y.; Salitra, G.; Kim, H. J.; Choi, S. Studies of Cycling Behavior, Ageing, and Interfacial Reactions of LiNi0.5Mn1.5O4 and Carbon Electrodes for Lithium-Ion 5-V Cells. *J. Power Sources* **2006**, *162* (2), 780−789.
(15) Li, T.; Yuan, X.-Z.; Zhang, L.; Song, D.; Shi, K.; Bock, C. Degradation Mechanisms and Mitigation Strategies of Nickel-Rich NMC-Based Lithium-Ion Batteries. *Electrochem. Energy Rev.* **2020**, *3* (1), 43−80.
(16) Sun, H. H.; Manthiram, A. Impact of Microcrack Generation and Surface Degradation on a Nickel-Rich Layered Li-[Ni0.9Co0.05Mn0.05]O2 Cathode for Lithium-Ion Batteries. *Chem. Mater.* **2017**, *29* (19), 8486−8493.
(17) Langdon, J.; Cui, Z.; Manthiram, A. Role of Electrolyte in Overcoming the Challenges of LiNiO2Cathode in Lithium Batteries. *ACS Energy Lett.* **2021**, *6* (11), 3809−3816.
(18) Xia, S.; Mu, L.; Xu, Z.; Wang, J.; Wei, C.; Liu, L.; Pianetta, P.; Zhao, K.; Yu, X.; Lin, F.; Liu, Y. Chemomechanical Interplay of Layered Cathode Materials Undergoing Fast Charging in Lithium Batteries. *Nano Energy* **2018**, *53*, 753−762.
(19) Liu, H.; Wolfman, M.; Karki, K.; Yu, Y.-S.; Stach, E. A.; Cabana, J.; Chapman, K. W.; Chupas, P. J. Intergranular Cracking as a Major Cause of Long-Term Capacity Fading of Layered Cathodes. *Nano Lett.* **2017**, *17* (6), 3452−3457.
(20) Park, K. J.; Hwang, J. Y.; Ryu, H. H.; Maglia, F.; Kim, S. J.; Lamp, P.; Yoon, C. S.; Sun, Y. K. Degradation Mechanism of Ni-Enriched NCA Cathode for Lithium Batteries: Are Microcracks Really Critical? *ACS Energy Lett.* **2019**, *4* (6), 1394−1400.
(21) Wandt, J.; Freiberg, A.; Thomas, R.; Gorlin, Y.; Siebel, A.; Jung, R.; Gasteiger, H. A.; Tromp, M. Transition Metal Dissolution and Deposition in Li-Ion Batteries Investigated by Operando X-Ray Absorption Spectroscopy. *J. Mater. Chem. A* **2016**, *4* (47), 18300−18305.
(22) Li, W.; Dolocan, A.; Oh, P.; Celio, H.; Park, S.; Cho, J.; Manthiram, A. Dynamic Behaviour of Interphases and Its Implication on High-Energy-Density Cathode Materials in Lithium-Ion Batteries. *Nat. Commun.* **2017**, *8*, 14589.
(23) Su, C.-C.; He, M.; Amine, R.; Chen, Z.; Yu, Z.; Rojas, T.; Cheng, L.; Ngo, A. T.; Amine, K. Unveiling Decaying Mechanism through Quantitative Structure-Activity Relationship in Electrolytes for Lithium-Ion Batteries. *Nano Energy* **2021**, *83*, No. 105843.
(24) Alvarado, J.; Schroeder, M. A.; Zhang, M.; Borodin, O.; Gobrogge, E.; Olguin, M.; Ding, M. S.; Gobet, M.; Greenbaum, S.; Meng, Y. S.; Xu, K. A Carbonate-Free, Sulfone-Based Electrolyte for High-Voltage Li-Ion Batteries. *Mater. Today* **2018**, *21* (4), 341−353.
(25) Yu, Y.; Karayaylali, P.; Katayama, Y.; Giordano, L.; Gauthier, M.; Maglia, F.; Jung, R.; Lund, I.; Shao-Horn, Y. Coupled LiPF6 Decomposition and Carbonate Dehydrogenation Enhanced by Highly Covalent Metal Oxides in High-Energy Li-Ion Batteries. *J. Phys. Chem. C* **2018**, *122* (48), 27368−27382.
(26) Zhang, Y.; Katayama, Y.; Tatara, R.; Giordano, L.; Yu, Y.; Fraggedakis, D.; Sun, J. G.; Maglia, F.; Jung, R.; Bazant, M. Z.; Shao-Horn, Y. Revealing Electrolyte Oxidation: Via Carbonate Dehydrogenation on Ni-Based Oxides in Li-Ion Batteries by in Situ Fourier Transform Infrared Spectroscopy. *Energy Environ. Sci.* **2020**, *13* (1), 183−199.
(27) Rinkel, B. L. D.; Hall, D. S.; Temprano, I.; Grey, C. P. Electrolyte Oxidation Pathways in Lithium-Ion Batteries. *J. Am. Chem. Soc.* **2020**, *142* (35), 15058−15074.
(28) Wang, C.; Xing, L.; Vatamanu, J.; Chen, Z.; Lan, G.; Li, W.; Xu, K. Overlooked Electrolyte Destabilization by Manganese (II) in Lithium-Ion Batteries. *Nat. Commun.* **2019**, *10* (1), 3423.
(29) Leung, K.; Rosy; Noked, M. Anodic Decomposition of Surface Films on High Voltage Spinel Surfaces - Density Function Theory and Experimental Study. *J. Chem. Phys.* **2019**, *151* (23), No. 234713.
(30) Pieczonka, N. P. W.; Liu, Z.; Lu, P.; Olson, K. L.; Moote, J.; Powell, B. R.; Kim, J. H. Understanding Transition-Metal Dissolution Behavior in LiNi 0.5Mn1.5O4 High-Voltage Spinel for Lithium Ion Batteries. *J. Phys. Chem. C* **2013**, *117* (31), 15947−15957.
(31) Kasnatscheew, J.; Röser, S.; Börner, M.; Winter, M. Do Increased Ni Contents in LiNi XMn YCo ZO2 (NMC) Electrodes Decrease Structural and Thermal Stability of Li Ion Batteries? A Thorough Look by Consideration of the Li+ Extraction Ratio. *ACS Appl. Energy Mater.* **2019**, *2* (11), 7733−7737.
(32) Aurbach, D.; Daroux, M.; Faguy, P.; Yeager, E. The Electrochemistry of Noble Metal Electrodes in Aprotic Organic Solvents Containing Lithium Salts. *J. Electroanal. Chem.* **1991**, *297* (1), 225−244.
(33) Edström, K.; Gustafsson, T.; Thomas, J. O. The Cathode-Electrolyte Interface in the Li-Ion Battery. *Electrochim. Acta* **2004**, *50*, 397−403.
(34) Aurbach, D. Review of Selected Electrode-Solution Interactions Which Determine the Performance of Li and Li Ion Batteries. *J. Power Sources* **2000**, *89* (2), 206−218.
(35) Yabuuchi, N.; Yoshii, K.; Myung, S.-T.; Nakai, I.; Komaba, S. Detailed Studies of a High-Capacity Electrode Material for Rechargeable Batteries, Li2MnO3−LiCo1/3Ni1/3Mn1/3O2. *J. Am. Chem. Soc.* **2011**, *133* (12), 4404−4419.
(36) Ma, J.; Hu, P.; Cui, G.; Chen, L. Surface and Interface Issues in Spinel LiNi0.5Mn1.5O4: Insights into a Potential Cathode Material for High Energy Density Lithium Ion Batteries. *Chem. Mater.* **2016**, *28* (11), 3578−3606.
(37) Talyosef, Y.; Markovsky, B.; Salitra, G.; Aurbach, D.; Kim, H. J.; Choi, S. The Study of LiNi0.5Mn1.5O4 5-V Cathodes for Li-Ion Batteries. *J. Power Sources* **2005**, *146*, 664−669.
(38) Peterson, S. W.; Wheeler, D. R. Direct Measurements of Effective Electronic Transport in Porous Li-Ion Electrodes. *J. Electrochem. Soc.* **2014**, *161* (14), A2175−A2181.
(39) Zhang, X.; Kostecki, R.; Richardson, T. J.; Pugh, J. K.; Ross, P. N. Electrochemical and Infrared Studies of the Reduction of Organic Carbonates. *J. Electrochem. Soc.* **2001**, *148* (12), A1341.
(40) Peled, E. The Electrochemical Behavior of Alkali and Alkaline Earth Metals in Nonaqueous Battery Systems—The Solid Electrolyte Interphase Model. *J. Electrochem. Soc.* **1979**, *126* (12), 2047−2051.
(41) Gauthier, M.; Carney, T. J.; Grimaud, A.; Giordano, L.; Pour, N.; Chang, H. H.; Fenning, D. P.; Lux, S. F.; Paschos, O.; Bauer, C.; Maglia, F.; Lupart, S.; Lamp, P.; Shao-Horn, Y. Electrode-Electrolyte Interface in Li-Ion Batteries: Current Understanding and New Insights. *J. Phys. Chem. Lett.* **2015**, *6*, 4653−4672.
(42) Yu, X.; Manthiram, A. Electrode-Electrolyte Interfaces in Lithium-Based Batteries. *Energy and Environmental Science.* **2018**, *11*, 527−543.
(43) Peled, E.; Menkin, S. Review—SEI: Past, Present and Future. *J. Electrochem. Soc.* **2017**, *164* (7), A1703−A1719.
(44) Xu, K. *Electrolytes, Interfaces and Interphases*, 1st ed.; Royal Society of Chemistry: Croydon, UK, 2023; DOI: 10.1039/9781837671311.
(45) Spotte-Smith, E. W. C.; Kam, R. L.; Barter, D.; Xie, X.; Hou, T.; Dwaraknath, S.; Blau, S. M.; Persson, K. A. Toward a Mechanistic Model of Solid-Electrolyte Interphase Formation and Evolution in Lithium-Ion Batteries. *ACS Energy Lett.* **2022**, *7* (4), 1446−1453.
(46) Kumar, R.; Tokranov, A.; Sheldon, B. W.; Xiao, X.; Huang, Z.; Li, C.; Mueller, T. In Situ and Operando Investigations of Failure Mechanisms of the Solid Electrolyte Interphase on Silicon Electrodes. *ACS Energy Lett.* **2016**, *1* (4), 689−697.
(47) Lee, S. H.; Hwang, J. Y.; Ming, J.; Kim, H.; Jung, H. G.; Sun, Y. K. Long-Lasting Solid Electrolyte Interphase for Stable Li-Metal Batteries. *ACS Energy Lett.* **2021**, *6* (6), 2153−2161.
(48) Dong, K.; Xu, Y.; Tan, J.; Osenberg, M.; Sun, F.; Kochovski, Z.; Pham, D. T.; Mei, S.; Hilger, A.; Ryan, E.; Lu, Y.; Banhart, J.; Manke, I. Unravelling the Mechanism of Lithium Nucleation and Growth and

the Interaction with the Solid Electrolyte Interface. *ACS Energy Lett.* **2021**, *6* (5), 1719−1728.
(49) Thomas, M. G. S. R.; Bruce, P. G.; Goodenough, J. B. AC Impedance Analysis of Polycrystalline Insertion Electrodes: Application to Li1 − x CoO2. *J. Electrochem. Soc.* **1985**, *132* (7), 1521−1528.
(50) Kanamura, K.; Toriyama, S.; Shiraishi, S.; Ohashi, M.; Takehara, Z. I. Studies on Electrochemical Oxidation of Non-Aqueous Electrolyte on the LiCoO2 Thin Film Electrode. *J. Electroanal. Chem.* **1996**, *419* (1), 77−84.
(51) Aurbach, D.; Levi, M. D.; Levi, E.; Teller, H.; Markovsky, B.; Salitra, G.; Heider, U.; Heider, L. Common Electroanalytical Behavior of Li Intercalation Processes into Graphite and Transition Metal Oxides. *J. Electrochem. Soc.* **1998**, *145* (9), 3024−3034.
(52) Aurbach, D.; Gamolsky, K.; Markovsky, B.; Salitra, G.; Gofer, Y.; Heider, U.; Oesten, R.; Schmidt, M. The Study of Surface Phenomena Related to Electrochemical Lithium Intercalation into Li[Sub x]MO[Sub y] Host Materials (M = Ni, Mn). *J. Electrochem. Soc.* **2000**, *147* (4), 1322.
(53) Eriksson, T.; Andersson, A. M.; Gejke, C.; Gustafsson, T.; Thomas, J. O. Influence of Temperature on the Interface Chemistry of LixMn2O4 Electrodes. *Langmuir* **2002**, *18* (9), 3609−3619.
(54) Rinkel, B. L. D.; Vivek, J. P.; Garcia-Araez, N.; Grey, C. P. Two Electrolyte Decomposition Pathways at Nickel-Rich Cathode Surfaces in Lithium-Ion Batteries. *Energy Environ. Sci.* **2022**, *15* (8), 3416−3438.
(55) Hestenes, J. C.; May, R.; Sadowski, J. T.; Munich, N.; Marbella, L. E. Resolving Chemical and Spatial Heterogeneities at Complex Electrochemical Interfaces in Li-Ion Batteries. *Chem. Mater.* **2022**, *34* (1), 232−243.
(56) Giordano, L.; Karayaylali, P.; Yu, Y.; Katayama, Y.; Maglia, F.; Lux, S.; Shao-Horn, Y. Chemical Reactivity Descriptor for the Oxide-Electrolyte Interface in Li-Ion Batteries. *J. Phys. Chem. Lett.* **2017**, *8* (16), 3881−3887.
(57) Østergaard, T. M.; Giordano, L.; Castelli, I. E.; Maglia, F.; Antonopoulos, B. K.; Shao-Horn, Y.; Rossmeisl, J. Oxidation of Ethylene Carbonate on Li Metal Oxide Surfaces. *J. Phys. Chem. C* **2018**, *122* (19), 10442−10449.
(58) Oswald, S.; Gasteiger, H. A. The Structural Stability Limit of Layered Lithium Transition Metal Oxides Due to Oxygen Release at High State of Charge and Its Dependence on the Nickel Content. *J. Electrochem. Soc.* **2023**, *170* (3), No. 030506.
(59) Teufl, T.; Strehle, B.; Müller, P.; Gasteiger, H. A.; Mendez, M. A. Oxygen Release and Surface Degradation of Li- and Mn-Rich Layered Oxides in Variation of the Li 2 MnO 3 Content. *J. Electrochem. Soc.* **2018**, *165* (11), A2718−A2731.
(60) Metzger, M.; Marino, C.; Sicklinger, J.; Haering, D.; Gasteiger, H. A. Anodic Oxidation of Conductive Carbon and Ethylene Carbonate in High-Voltage Li-Ion Batteries Quantified by On-Line Electrochemical Mass Spectrometry. *J. Electrochem. Soc.* **2015**, *162* (7), A1123−A1134.
(61) Jung, R.; Metzger, M.; Maglia, F.; Stinner, C.; Gasteiger, H. A. Chemical versus Electrochemical Electrolyte Oxidation on NMC111, NMC622, NMC811, LNMO, and Conductive Carbon. *J. Phys. Chem. Lett.* **2017**, *8* (19), 4820−4825.
(62) Borodin, O.; Behl, W.; Jow, T. R. Oxidative Stability and Initial Decomposition Reactions of Carbonate, Sulfone, and Alkyl Phosphate-Based Electrolytes. *J. Phys. Chem. C* **2013**, *117* (17), 8661−8682.
(63) Li, T.; Xing, L.; Li, W.; Wang, Y.; Xu, M.; Gu, F.; Hu, S. How Does Lithium Salt Anion Affect Oxidation Decomposition Reaction of Ethylene Carbonate: A Density Functional Theory Study. *J. Power Sources* **2013**, *244*, 668−674.
(64) Renfrew, S. E.; McCloskey, B. D. Quantification of Surface Oxygen Depletion and Solid Carbonate Evolution on the First Cycle of LiNi0.6Mn0.2Co0.2O2 Electrodes. *ACS Appl. Energy Mater.* **2019**, *2* (5), 3762−3772.
(65) Freiberg, A. T. S.; Sicklinger, J.; Solchenbach, S.; Gasteiger, H. A. Li2CO3 Decomposition in Li-Ion Batteries Induced by the Electrochemical Oxidation of the Electrolyte and of Electrolyte Impurities. *Electrochim. Acta* **2020**, *346*, No. 136271.
(66) Benedek, R.; Thackeray, M. M. Reaction Energy for LiMn 2O 4 Spinel Dissolution in Acid. *Electrochem. Solid-State Lett.* **2006**, *9* (6), A265−A267.
(67) Solchenbach, S.; Metzger, M.; Egawa, M.; Beyer, H.; Gasteiger, H. A. Quantification of PF5 and POF3 from Side Reactions of LiPF6 in Li-Ion Batteries. *J. Electrochem. Soc.* **2018**, *165* (13), A3022.
(68) Hestenes, J. C.; Sadowski, J. T.; May, R.; Marbella, L. E. Transition Metal Dissolution Mechanisms and Impacts on Electronic Conductivity in Composite LiNi0.5Mn1.5O4Cathode Films. *ACS Mater. Au* **2023**, *3* (2), 88−101.
(69) Yoon, T.; Kim, D.; Park, K. H.; Park, H.; Jurng, S.; Jang, J.; Ryu, J. H.; Kim, J. J.; Oh, S. M. Compositional Change of Surface Film Deposited on LiNi 0.5 Mn 1.5 O 4 Positive Electrode. *J. Electrochem. Soc.* **2014**, *161* (4), A519−A523.
(70) Teng, X.; Zhan, C.; Bai, Y.; Ma, L.; Liu, Q.; Wu, C.; Wu, F.; Yang, Y.; Lu, J.; Amine, K. In Situ Analysis of Gas Generation in Lithium-Ion Batteries with Different Carbonate-Based Electrolytes. *ACS Appl. Mater. Interfaces* **2015**, *7* (41), 22751−22755.
(71) Yoon, T.; Lee, T.; Soon, J.; Jeong, H.; Jurng, S.; Ryu, J. H.; Oh, S. M. The Investigation of Electrolyte Oxidation and Film Deposition Characteristics at High Potentials in a Carbonate-Based Electrolyte Using Pt Electrode. *J. Electrochem. Soc.* **2018**, *165* (5), A1095−A1098.
(72) Yoon, T.; Soon, J.; Lee, T. J.; Ryu, J. H.; Oh, S. M. Dissolution of Cathode−Electrolyte Interphase Deposited on LiNi0.5Mn1.5O4 for Lithium-Ion Batteries. *J. Power Sources* **2021**, *503*, No. 230051.
(73) Zhang, J. N.; Li, Q.; Wang, Y.; Zheng, J.; Yu, X.; Li, H. Dynamic Evolution of Cathode Electrolyte Interphase (CEI) on High Voltage LiCoO2 Cathode and Its Interaction with Li Anode. *Energy Storage Mater.* **2018**, *14*, 1−7.
(74) Fang, S.; Jackson, D.; Dreibelbis, M. L.; Kuech, T. F.; Hamers, R. J. Anode-Originated SEI Migration Contributes to Formation of Cathode-Electrolyte Interphase Layer. *J. Power Sources* **2018**, *373*, 184−192.
(75) Cuisinier, M.; Dupré, N.; Martin, J. F.; Kanno, R.; Guyomard, D. Evolution of the LiFePO4 Positive Electrode Interface along Cycling Monitored by MAS NMR. *J. Power Sources* **2013**, *224*, 50−58.
(76) Kühn, S. P.; Edström, K.; Winter, M.; Cekic-Laskovic, I. Face to Face at the Cathode Electrolyte Interphase: From Interface Features to Interphase Formation and Dynamics. *Adv. Mater. Interfaces* **2022**, *9* (8), 2102078.
(77) Okuno, Y.; Ushirogata, K.; Sodeyama, K.; Shukri, G.; Tateyama, Y. Structures, Electronic States, and Reactions at Interfaces between LiNi 0.5 Mn 1.5 O 4 Cathode and Ethylene Carbonate Electrolyte: A First-Principles Study. *J. Phys. Chem. C* **2019**, *123* (4), 2267−2277.
(78) Li, J.; Manthiram, A. A Comprehensive Analysis of the Interphasial and Structural Evolution over Long-Term Cycling of Ultrahigh-Nickel Cathodes in Lithium-Ion Batteries. *Adv. Energy Mater.* **2019**, *9* (45), No. 1902731.
(79) Zhang, Y.; Kim, C. S.; Song, H. W.; Chang, S. J.; Kim, H.; Park, J.; Hu, S.; Zhao, K.; Lee, S. Ultrahigh Active Material Content and Highly Stable Ni-Rich Cathode Leveraged by Oxidative Chemical Vapor Deposition. *Energy Storage Mater.* **2022**, *48*, 1−11.
(80) Atkins, D.; Ayerbe, E.; Benayad, A.; Capone, F. G.; Capria, E.; Castelli, I. E.; Cekic-Laskovic, I.; Ciria, R.; Dudy, L.; Edström, K.; Johnson, M. R.; Li, H.; Lastra, J. M. G.; De Souza, M. L.; Meunier, V.; Morcrette, M.; Reichert, H.; Simon, P.; Rueff, J. P.; Sottmann, J.; Wenzel, W.; Grimaud, A. Understanding Battery Interfaces by Combined Characterization and Simulation Approaches: Challenges and Perspectives. *Adv. Energy Mater.* **2022**, *12* (17), No. 2102687.
(81) Sungjemmenla; S. K., V.; Soni, C. B.; Kumar, V.; Seh, Z. W. Understanding the Cathode−Electrolyte Interphase in Lithium-Ion Batteries. *Energy Technol.* **2022**, *10*, 2200421.
(82) Zhang, Z.; Wang, X.; Bai, Y.; Wu, C. Charactering and Optimizing Cathode Electrolytes Interface for Advanced Rechargeable Batteries: Promises and Challenges. *Green Energy Environ.* **2022**, *7* (4), 606−635.

https://doi.org/10.1021/acsenergylett.3c01529
ACS Energy Lett. 2023, 8, 4572−4596

(83) Chou, H.; Ismach, A.; Ghosh, R.; Ruoff, R. S.; Dolocan, A. Revealing the Planar Chemistry of Two-Dimensional Heterostructures at the Atomic Level. *Nat. Commun.* **2015**, *6* (1), 7482.
(84) Chen, Y.; Zhao, W.; Zhang, Q.; Yang, G.; Zheng, J.; Tang, W.; Xu, Q.; Lai, C.; Yang, J.; Peng, C. Armoring LiNi1/3Co1/3Mn1/3O2 Cathode with Reliable Fluorinated Organic−Inorganic Hybrid Interphase Layer toward Durable High Rate Battery. *Adv. Funct. Mater.* **2020**, *30* (19), No. 2000396.
(85) Zhao, D.; Wang, J.; Lu, H.; Wang, P.; Liu, H.; Li, S. Tailoring Interfacial Architecture of High-Voltage Cathode with Lithium Difluoro(Bisoxalato) Phosphate for High Energy Density Battery. *J. Power Sources* **2020**, *456*, No. 228006.
(86) Cui, Z.; Xie, Q.; Manthiram, A. A Cobalt- and Manganese-Free High-Nickel Layered Oxide Cathode for Long-Life, Safer Lithium-Ion Batteries. *Adv. Energy Mater.* **2021**, *11* (41), No. 2102421.
(87) Sheng, H.; Meng, X. H.; Xiao, D. D.; Fan, M.; Chen, W. P.; Wan, J.; Tang, J.; Zou, Y. G.; Wang, F.; Wen, R.; Shi, J. L.; Guo, Y. G. An Air-Stable High-Nickel Cathode with Reinforced Electrochemical Performance Enabled by Convertible Amorphous Li2CO3Modification. *Adv. Mater.* **2022**, *34* (12), No. 2108947.
(88) Ma, L.; Ellis, L.; Glazier, S. L.; Ma, X.; Dahn, J. R. Combinations of LiPO 2 F 2 and Other Electrolyte Additives in Li[Ni 0.5 Mn 0.3 Co 0.2]O 2 /Graphite Pouch Cells. *J. Electrochem. Soc.* **2018**, *165* (9), A1718−A1724.
(89) He, M.; Guo, R.; Hobold, G. M.; Gao, H.; Gallant, B. M. The Intrinsic Behavior of Lithium Fluoride in Solid Electrolyte Interphases on Lithium. *Proc. Natl. Acad. Sci. U. S. A.* **2020**, *117* (1), 73−79.
(90) Dupré, N.; Martin, J. F.; Oliveri, J.; Soudan, P.; Yamada, A.; Kanno, R.; Guyomard, D. Relationship between Surface Chemistry and Electrochemical Behavior of LiNi1/2Mn1/2O2 Positive Electrode in a Lithium-Ion Battery. *J. Power Sources* **2011**, *196* (10), 4791−4800.
(91) Dupré, N.; Martin, J. F.; Guyomard, D.; Yamada, A.; Kanno, R. Detection of Surface Layers Using 7Li MAS NMR. *J. Mater. Chem.* **2008**, *18* (36), 4266−4273.
(92) Grey, C. P.; Dupré, N. NMR Studies of Cathode Materials for Lithium-Ion Rechargeable Batteries. *Chem. Rev.* **2004**, *104* (10), 4493−4512.
(93) Hestenes, J. C.; Ells, A. W.; Navarro Goldaraz, M.; Sergeyev, I. V.; Itin, B.; Marbella, L. E. Reversible Deposition and Stripping of the Cathode Electrolyte Interphase on Li2RuO3. *Front. Chem.* **2020**, *8*, 681.
(94) Yu, Y.; Karayaylali, P.; Nowak, S. H.; Giordano, L.; Gauthier, M.; Hong, W.; Kou, R.; Li, Q.; Vinson, J.; Kroll, T.; Sokaras, D.; Sun, C. J.; Charles, N.; Maglia, F.; Jung, R.; Shao-Horn, Y. Revealing Electronic Signatures of Lattice Oxygen Redox in Lithium Ruthenates and Implications for High-Energy Li-Ion Battery Material Designs. *Chem. Mater.* **2019**, *31* (19), 7864−7876.
(95) Jay, R.; Jadhav, A. L.; Gordon, L. W.; Messinger, R. J. Soluble Electrolyte-Coordinated Sulfide Species Revealed in Al-S Batteries by Nuclear Magnetic Resonance Spectroscopy. *Chem. Mater.* **2022**, *2022*, 44.
(96) Diercks, D. R.; Musselman, M.; Morgenstern, A.; Wilson, T.; Kumar, M.; Smith, K.; Kawase, M.; Gorman, B. P.; Eberhart, M.; Packard, C. E. Evidence for Anisotropic Mechanical Behavior and Nanoscale Chemical Heterogeneity in Cycled LiCoO 2. *J. Electrochem. Soc.* **2014**, *161* (11), F3039−F3045.
(97) Maier, J.; Pfeiffer, B.; Volkert, C. A.; Nowak, C. Three-Dimensional Microstructural Characterization of Lithium Manganese Oxide with Atom Probe Tomography. *Energy Technol.* **2016**, *4* (12), 1565−1574.
(98) Devaraj, A.; Gu, M.; Colby, R.; Yan, P.; Wang, C. M.; Zheng, J. M.; Xiao, J.; Genc, A.; Zhang, J. G.; Belharouak, I.; Wang, D.; Amine, K.; Thevuthasan, S. Visualizing Nanoscale 3D Compositional Fluctuation of Lithium in Advanced Lithium-Ion Battery Cathodes. *Nat. Commun.* **2015**, *6* (1), 8014.
(99) Scipioni, R.; Isheim, D.; Barnett, S. A. Revealing the Complex Layered-Mosaic Structure of the Cathode Electrolyte Interphase in Li-Ion Batteries. *Appl. Mater. Today* **2020**, *20*, No. 100748.
(100) Erickson, E. M.; Li, W.; Dolocan, A.; Manthiram, A. Insights into the Cathode-Electrolyte Interphases of High-Energy-Density Cathodes in Lithium-Ion Batteries. *ACS Appl. Mater. Interfaces* **2020**, *12* (14), 16451−16461.
(101) Li, T.; Devaraj, A.; Kruse, N. Atomic-Scale Characterization of (Electro-)Catalysts and Battery Materials by Atom Probe Tomography. *Cell Rep. Phys. Sci.* **2022**, *3*, No. 101188.
(102) Wandt, J.; Freiberg, A. T. S.; Ogrodnik, A.; Gasteiger, H. A. Singlet Oxygen Evolution from Layered Transition Metal Oxide Cathode Materials and Its Implications for Lithium-Ion Batteries. *Mater. Today* **2018**, *21* (8), 825−833.
(103) Yusuf, A.; Sai Avvaru, V.; De la Vega, J.; Zhang, M.; Garcia Molleja, J.; Wang, D. Y. Unveiling the Structure, Chemistry, and Formation Mechanism of an in-Situ Phosphazene Flame Retardant-Derived Interphase Layer in LiFePO4 Cathode. *Chem. Eng. J.* **2023**, *455*, No. 140678.
(104) Zhu, Y.; Zhu, J.; Jiang, B.; Wang, X.; Wei, X.; Dai, H. Insights on the Degradation Mechanism for Large Format Prismatic Graphite/LiFePO4 Battery Cycled under Elevated Temperature. *J. Energy Storage* **2023**, *60*, No. 106624.
(105) Logan, E. R.; Hebecker, H.; Eldesoky, A.; Luscombe, A.; Johnson, M. B.; Dahn, J. R. Performance and Degradation of LiFePO 4 /Graphite Cells: The Impact of Water Contamination and an Evaluation of Common Electrolyte Additives. *J. Electrochem. Soc.* **2020**, *167* (13), 130543.
(106) Zuo, T. T.; Walther, F.; Ahmed, S.; Rueß, R.; Hertle, J.; Mogwitz, B.; Volz, K.; Janek, J. Formation of an Artificial Cathode-Electrolyte Interphase to Suppress Interfacial Degradation of Ni-Rich Cathode Active Material with Sulfide Electrolytes for Solid-State Batteries. *ACS Energy Lett.* **2023**, *8* (3), 1322−1329.
(107) Chen, M.; Ma, C.; Ding, Z.; Zhou, L.; Chen, L.; Gao, P.; Wei, W. Upgrading Electrode/Electrolyte Interphases via Polyamide-Based Quasi-Solid Electrolyte for Long-Life Nickel-Rich Lithium Metal Batteries. *ACS Energy Lett.* **2021**, *6* (4), 1280−1289.
(108) Zhang, Z.; Yang, J.; Huang, W.; Wang, H.; Zhou, W.; Li, Y.; Li, Y.; Xu, J.; Huang, W.; Chiu, W.; Cui, Y. Cathode-Electrolyte Interphase in Lithium Batteries Revealed by Cryogenic Electron Microscopy. *Matter* **2021**, *4* (1), 302−312.
(109) Wang, X.; Zhang, M.; Alvarado, J.; Wang, S.; Sina, M.; Lu, B.; Bouwer, J.; Xu, W.; Xiao, J.; Zhang, J. G.; Liu, J.; Meng, Y. S. New Insights on the Structure of Electrochemically Deposited Lithium Metal and Its Solid Electrolyte Interphases via Cryogenic TEM. *Nano Lett.* **2017**, *17* (12), 7606−7612.
(110) Wu, Y.; Feng, X.; Liu, X.; Wang, X.; Ren, D.; Wang, L.; Yang, M.; Wang, Y.; Zhang, W.; Li, Y.; Zheng, Y.; Lu, L.; Han, X.; Xu, G. L.; Ren, Y.; Chen, Z.; Chen, J.; He, X.; Amine, K.; Ouyang, M. In-Built Ultraconformal Interphases Enable High-Safety Practical Lithium Batteries. *Energy Storage Mater.* **2021**, *43*, 248−257.
(111) Holoubek, J.; Yan, Q.; Liu, H.; Hopkins, E. J.; Wu, Z.; Yu, S.; Luo, J.; Pascal, T. A.; Chen, Z.; Liu, P. Oxidative Stabilization of Dilute Ether Electrolytes via Anion Modification. *ACS Energy Lett.* **2022**, *7* (2), 675−682.
(112) Zhang, Q.; Ma, J.; Mei, L.; Liu, J.; Li, Z.; Li, J.; Zeng, Z. In Situ TEM Visualization of LiF Nanosheet Formation on the Cathode-Electrolyte Interphase (CEI) in Liquid-Electrolyte Lithium-Ion Batteries. *Matter* **2022**, *5* (4), 1235−1250.
(113) Wang, X.; Li, Y.; Meng, Y. S. Cryogenic Electron Microscopy for Characterizing and Diagnosing Batteries. *Joule* **2018**, *2* (11), 2225−2234.
(114) Han, B.; Zhang, Z.; Zou, Y.; Xu, K.; Xu, G.; Wang, H.; Meng, H.; Deng, Y.; Li, J.; Gu, M. Poor Stability of Li2CO3 in the Solid Electrolyte Interphase of a Lithium-Metal Anode Revealed by Cryo-Electron Microscopy. *Adv. Mater.* **2021**, *33* (22), No. 2100404.
(115) Yan, Y.; Weng, S.; Fu, A.; Zhang, H.; Chen, J.; Zheng, Q.; Zhang, B.; Zhou, S.; Yan, H.; Wang, C. W.; Tang, Y.; Luo, H.; Mao, B. W.; Zheng, J.; Wang, X.; Qiao, Y.; Yang, Y.; Sun, S. G. Tailoring Electrolyte Dehydrogenation with Trace Additives: Stabilizing the LiCoO2Cathode beyond 4.6 V. *ACS Energy Lett.* **2022**, *7* (8), 2677−2684.

https://doi.org/10.1021/acsenergylett.3c01529
ACS Energy Lett. 2023, 8, 4572−4596

(116) Zhu, W.; Huang, X.; Liu, T.; Xie, Z.; Wang, Y.; Tian, K.; Bu, L.; Wang, H.; Gao, L.; Zhao, J. Ultrathin Al2O3 Coating on LiNi0.8Co0.1Mn0.1O2 Cathode Material for Enhanced Cycleability at Extended Voltage Ranges. *Coatings* **2019**, *9* (2), 92.
(117) Mohanty, D.; Dahlberg, K.; King, D. M.; David, L. A.; Sefat, A. S.; Wood, D. L.; Daniel, C.; Dhar, S.; Mahajan, V.; Lee, M.; Albano, F. Modification of Ni-Rich FCG NMC and NCA Cathodes by Atomic Layer Deposition: Preventing Surface Phase Transitions for High-Voltage Lithium-Ion Batteries. *Sci. Rep.* **2016**, *6*, 26532.
(118) Mirolo, M.; Vaz, C. A. F.; Novák, P.; El Kazzi, M. Multi-Length-Scale x-Ray Spectroscopies for Determination of Surface Reactivity at High Voltages of LiNi0.8Co0.15Al0.05O2vs Li4Ti5O12. *J. Chem. Phys.* **2020**, *152* (18), No. 184705.
(119) Leanza, D.; Vaz, C. A. F.; Melinte, G.; Mu, X.; Novák, P.; El Kazzi, M. Revealing the Dual Surface Reactions on a HE-NCM Li-Ion Battery Cathode and Their Impact on the Surface Chemistry of the Counter Electrode. *ACS Appl. Mater. Interfaces* **2019**, *11* (6), 6054−6065.
(120) Leanza, D.; Vaz, C. A. F.; Novák, P.; El Kazzi, M. Instability of PVDF Binder in the LiFePO4 versus Li4Ti5O12 Li-Ion Battery Cell. *Helv. Chim. Acta* **2021**, *104* (1), No. e2000183.
(121) Mirolo, M.; Leanza, D.; Höltschi, L.; Jordy, C.; Pelé, V.; Novák, P.; El Kazzi, M.; Vaz, C. A. F. Post Mortem and Operando XPEEM: A Surface-Sensitive Tool for Studying Single Particles in Li-Ion Battery Composite Electrodes. *Anal. Chem.* **2020**, *92* (4), 3023−3031.
(122) Matsui, M.; Dokko, K.; Akita, Y.; Munakata, H.; Kanamura, K. Surface Layer Formation of LiCoO 2 Thin Film Electrodes in Non-Aqueous Electrolyte Containing Lithium Bis(Oxalate)Borate. *J. Power Sources* **2012**, *210*, 60−66.
(123) Akita, Y.; Segawa, M.; Munakata, H.; Kanamura, K. In-Situ Fourier Transform Infrared Spectroscopic Analysis on Dynamic Behavior of Electrolyte Solution on LiFePO4 Cathode. *J. Power Sources* **2013**, *239*, 175−180.
(124) Kanamura, K.; Umegaki, T.; Ohashi, M.; Toriyama, S.; Shiraishi, S.; Takehara, Z.-i. Oxidation of Propylene Carbonate Containing LiBF4 or LiPF6 on LiCoO2 Thin Film Electrode for Lithium Batteries. *Electrochim. Acta* **2001**, *47* (3), 433−439.
(125) Matsushita, T.; Dokko, K.; Kanamura, K. In Situ FT-IR Measurement for Electrochemical Oxidation of Electrolyte with Ethylene Carbonate and Diethyl Carbonate on Cathode Active Material Used in Rechargeable Lithium Batteries. *J. Power Sources* **2005**, *146*, 360−364.
(126) Yamamoto, K.; Minato, T.; Mori, S.; Takamatsu, D.; Orikasa, Y.; Tanida, H.; Nakanishi, K.; Murayama, H.; Masese, T.; Mori, T.; Arai, H.; Koyama, Y.; Ogumi, Z.; Uchimoto, Y. Improved Cyclic Performance of Lithium-Ion Batteries: An Investigation of Cathode/Electrolyte Interface via in Situ Total-Reflection Fluorescence X-Ray Absorption Spectroscopy. *J. Phys. Chem. C* **2014**, *118* (18), 9538−9543.
(127) Sharabi, R.; Markevich, E.; Borgel, V.; Salitra, G.; Aurbach, D.; Semrau, G.; Schmidt, M. A. In Situ FTIR Spectroscopy Study of Li/LiNi0.8Co 0.15Al0.05O2 Cells with Ionic Liquid-Based Electrolytes in Overcharge Condition. *Electrochem. Solid-State Lett.* **2010**, *13* (4), A32.
(128) Suo, L.; Borodin, O.; Gao, T.; Olguin, M.; Ho, J.; Fan, X.; Luo, C.; Wang, C.; Xu, K. Water-in-Salt" Electrolyte Enables High-Voltage Aqueous Lithium-Ion Chemistries. *Science (80-.).* **2015**, *350* (6263), 938−943.
(129) Meng, Y.; Chen, G.; Shi, L.; Liu, H.; Zhang, D. Operando Fourier Transform Infrared Investigation of Cathode Electrolyte Interphase Dynamic Reversible Evolution on Li1.2Ni0.2Mn0.6O2. *ACS Appl. Mater. Interfaces* **2019**, *11* (48), 45108−45117.
(130) Weiling, M.; Pfeiffer, F.; Baghernejad, M. Vibrational Spectroscopy Insight into the Electrodelelectrolyte Interface/Interphase in Lithium Batteries. *Adv. Energy Mater.* **2022**, *12* (46), No. 2202504.
(131) Piernas-Muñoz, M. J.; Tornheim, A.; Trask, S.; Zhang, Z.; Bloom, I. Surface-Enhanced Raman Spectroscopy (SERS): A Powerful Technique to Study the SEI Layer in Batteries. *Chem. Commun.* **2021**, *57* (18), 2253−2256.
(132) Gajan, A.; Lecourt, C.; Torres Bautista, B. E.; Fillaud, L.; Demeaux, J.; Lucas, I. T. Solid Electrolyte Interphase Instability in Operating Lithium-Ion Batteries Unraveled by Enhanced-Raman Spectroscopy. *ACS Energy Lett.* **2021**, *6* (5), 1757−1763.
(133) Chen, D.; Mahmoud, M. A.; Wang, J. H.; Waller, G. H.; Zhao, B.; Qu, C.; El-Sayed, M. A.; Liu, M. Operando Investigation into Dynamic Evolution of Cathode-Electrolyte Interfaces in a Li-Ion Battery. *Nano Lett.* **2019**, *19* (3), 2037−2043.
(134) Pfeiffer, F.; Diddens, D.; Weiling, M.; Baghernejad, M. Study of a High-Voltage NMC Interphase in the Presence of a Thiophene Additive Realized by Operando SHINERS. *ACS Appl. Mater. Interfaces* **2023**, *15* (5), 6676−6686.
(135) Han, X. X.; Rodriguez, R. S.; Haynes, C. L.; Ozaki, Y.; Zhao, B. Surface-Enhanced Raman Spectroscopy. *Nat. Rev. Methods Primers* **2021**, *1*, 1−17.
(136) Hy, S.; Felix, F.; Rick, J.; Su, W. N.; Hwang, B. J. Direct in Situ Observation of Li2O Evolution on Li-Rich High-Capacity Cathode Material, Li[NixLi(1−2x)/3Mn (2-x)/3]O2 ($0 \leq x \leq 0.5$). *J. Am. Chem. Soc.* **2014**, *136* (3), 999−1007.
(137) Li, J. F.; Huang, Y. F.; Ding, Y.; Yang, Z. L.; Li, S. B.; Zhou, X. S.; Fan, F. R.; Zhang, W.; Zhou, Z. Y.; Wu, D. Y.; Ren, B.; Wang, Z. L.; Tian, Z. Q. Shell-Isolated Nanoparticle-Enhanced Raman Spectroscopy. *Nature* **2010**, *464* (7287), 392−395.
(138) Wiemers-Meyer, S.; Winter, M.; Nowak, S. A Battery Cell for in Situ NMR Measurements of Liquid Electrolytes. *Phys. Chem. Chem. Phys.* **2017**, *19* (7), 4962−4966.
(139) Gachot, G.; Grugeon, S.; Armand, M.; Pilard, S.; Guenot, P.; Tarascon, J. M.; Laruelle, S. Deciphering the Multi-Step Degradation Mechanisms of Carbonate-Based Electrolyte in Li Batteries. *J. Power Sources* **2008**, *178* (1), 409−421.
(140) Wang, L.; Menakath, A.; Han, F.; Wang, Y.; Zavalij, P. Y.; Gaskell, K. J.; Borodin, O.; Iuga, D.; Brown, S. P.; Wang, C.; Xu, K.; Eichhorn, B. W. Identifying the Components of the Solid−Electrolyte Interphase in Li-Ion Batteries. *Nat. Chem.* **2019**, *11* (9), 789−796.
(141) Pritzl, D.; Solchenbach, S.; Wetjen, M.; Gasteiger, H. A. Analysis of Vinylene Carbonate (VC) as Additive in Graphite/LiNi 0.5 Mn 1.5 O 4 Cells. *J. Electrochem. Soc.* **2017**, *164* (12), A2625−A2635.
(142) Stich, M.; Göttlinger, M.; Kurniawan, M.; Schmidt, U.; Bund, A. Hydrolysis of LiPF6 in Carbonate-Based Electrolytes for Lithium-Ion Batteries and in Aqueous Media. *J. Phys. Chem. C* **2018**, *122* (16), 8836−8842.
(143) Plakhotnyk, A. V.; Ernst, L.; Schmutzler, R. Hydrolysis in the System LiPF 6 - Propylene Carbonate - Dimethyl Carbonate - H 2O. *J. Fluor. Chem.* **2005**, *126* (1), 27−31.
(144) Guéguen, A.; Streich, D.; He, M.; Mendez, M.; Chesneau, F. F.; Novák, P.; Berg, E. J. Decomposition of LiPF 6 in High Energy Lithium-Ion Batteries Studied with Online Electrochemical Mass Spectrometry. *J. Electrochem. Soc.* **2016**, *163* (6), A1095−A1100.
(145) Gireaud, L.; Grugeon, S.; Laruelle, S.; Pilard, S.; Tarascon, J.-M. Identification of Li Battery Electrolyte Degradation Products Through Direct Synthesis and Characterization of Alkyl Carbonate Salts. *J. Electrochem. Soc.* **2005**, *152* (5), A850.
(146) Campion, C. L.; Li, W.; Lucht, B. L. Thermal Decomposition of LiPF[Sub 6]-Based Electrolytes for Lithium-Ion Batteries. *J. Electrochem. Soc.* **2005**, *152* (12), A2327.
(147) Allen, J. P.; O'Keefe, C. A.; Grey, C. P. Quantifying Dissolved Transition Metals in Battery Electrolyte Solutions with NMR Paramagnetic Relaxation Enhancement. *J. Phys. Chem. C* **2023**, *127*, 9509−9521.
(148) Metzger, M.; Gasteiger, H. A. Diagnosing Battery Degradation via Gas Analysis. *Energy Environ. Mater.* **2022**, *5* (3), 688−692.
(149) Jung, R.; Strobl, P.; Maglia, F.; Stinner, C.; Gasteiger, H. A. Temperature Dependence of Oxygen Release from LiNi 0.6 Mn 0.2 Co 0.2 O 2 (NMC622) Cathode Materials for Li-Ion Batteries. *J. Electrochem. Soc.* **2018**, *165* (11), A2869−A2879.

https://doi.org/10.1021/acsenergylett.3c01529
ACS Energy Lett. 2023, 8, 4572−4596

(150) Hatsukade, T.; Schiele, A.; Hartmann, P.; Brezesinski, T.; Janek, J. Origin of Carbon Dioxide Evolved during Cycling of Nickel-Rich Layered NCM Cathodes. *ACS Appl. Mater. Interfaces* **2018**, *10* (45), 38892−38899.
(151) Dose, W. M.; Li, W.; Temprano, I.; O'Keefe, C. A.; Mehdi, B. L.; De Volder, M. F. L.; Grey, C. P. Onset Potential for Electrolyte Oxidation and Ni-Rich Cathode Degradation in Lithium-Ion Batteries. *ACS Energy Lett.* **2022**, *7* (10), 3524−3530.
(152) Azcarate, I.; Yin, W.; Méthivier, C.; Ribot, F.; Laberty-Robert, C.; Grimaud, A. Assessing the Oxidation Behavior of EC:DMC Based Electrolyte on Non-Catalytically Active Surface. *J. Electrochem. Soc.* **2020**, *167* (8), No. 080530.
(153) Teufl, T.; Pritzl, D.; Krieg, P.; Strehle, B.; Mendez, M. A.; Gasteiger, H. A. Operating EC-Based Electrolytes with Li- and Mn-Rich NCMs: The Role of O 2 -Release on the Choice of the Cyclic Carbonate. *J. Electrochem. Soc.* **2020**, *167* (11), 110505.
(154) Dose, W. M.; Temprano, I.; Allen, J. P.; Björklund, E.; O'Keefe, C. A.; Li, W.; Mehdi, B. L.; Weatherup, R. S.; De Volder, M. F. L.; Grey, C. P. Electrolyte Reactivity at the Charged Ni-Rich Cathode Interface and Degradation in Li-Ion Batteries. *ACS Appl. Mater. Interfaces* **2022**, *14* (11), 13206−13222.
(155) Freiberg, A. T. S.; Roos, M. K.; Wandt, J.; De Vivie-Riedle, R.; Gasteiger, H. A. Singlet Oxygen Reactivity with Carbonate Solvents Used for Li-Ion Battery Electrolytes. *J. Phys. Chem. A* **2018**, *122* (45), 8828−8839.
(156) Dong, Y.; Demeaux, J.; Lucht, B. L. Investigation of the Effect of Added Methylene Ethylene Carbonate (MEC) and Vinylene Carbonate (VC) on LiNi 0.5 Mn 1.5 O 4 /Graphite Cell Performance. *J. Electrochem. Soc.* **2016**, *163* (10), A2413−A2417.
(157) Xie, Q.; Cui, Z.; Manthiram, A. Unveiling the Stabilities of Nickel-Based Layered Oxide Cathodes at an Identical Degree of Delithiation in Lithium-Based Batteries. *Adv. Mater.* **2021**, *33* (32), No. 2100804.
(158) Papp, J. K.; Li, N.; Kaufman, L. A.; Naylor, A. J.; Younesi, R.; Tong, W.; McCloskey, B. D. A Comparison of High Voltage Outgassing of LiCoO2, LiNiO2, and Li2MnO3 Layered Li-Ion Cathode Materials. *Electrochim. Acta* **2021**, *368*, No. 137505.
(159) Metzger, M.; Strehle, B.; Solchenbach, S.; Gasteiger, H. A. Origin of H 2 Evolution in LIBs: H 2 O Reduction vs. Electrolyte Oxidation. *J. Electrochem. Soc.* **2016**, *163* (5), A798−A809.
(160) Langdon, J.; Sim, R.; Manthiram, A. Gas Generation in Lithium Cells with High-Nickel Cathodes and Localized High-Concentration Electrolytes. *ACS Energy Lett.* **2022**, *7* (8), 2634−2640.
(161) Metzger, M.; Sicklinger, J.; Haering, D.; Kavakli, C.; Stinner, C.; Marino, C.; Gasteiger, H. A. Carbon Coating Stability on High-Voltage Cathode Materials in H 2 O-Free and H 2 O-Containing Electrolyte. *J. Electrochem. Soc.* **2015**, *162* (7), A1227−A1235.
(162) Heider, U.; Oesten, R.; Jungnitz, M. Challenge in Manufacturing Electrolyte Solutions for Lithium and Lithium Ion Batteries Quality Control and Minimizing Contamination Level. *J. Power Sources* **1999**, *81*−*82*, 119−122.
(163) Choi, W.; Manthiram, A. Comparison of Metal Ion Dissolutions from Lithium Ion Battery Cathodes. *J. Electrochem. Soc.* **2006**, *153* (9), A1760.
(164) Li, Q.; Wang, Y.; Wang, X.; Sun, X.; Zhang, J. N.; Yu, X.; Li, H. Investigations on the Fundamental Process of Cathode Electrolyte Interphase Formation and Evolution of High-Voltage Cathodes. *ACS Appl. Mater. Interfaces* **2020**, *12* (2), 2319−2326.
(165) Streich, D.; Erk, C.; Guéguen, A.; Müller, P.; Chesneau, F. F.; Berg, E. J. Operando Monitoring of Early Ni-Mediated Surface Reconstruction in Layered Lithiated Ni-Co-Mn Oxides. *J. Phys. Chem. C* **2017**, *121* (25), 13481−13486.
(166) Salomez, B.; Grugeon, S.; Armand, M.; Tran-Van, P.; Laruelle, S. Review—Gassing Mechanisms in Lithium-Ion Battery. *J. Electrochem. Soc.* **2023**, *170* (5), No. 050537.
(167) Xiong, D. J.; Ellis, L. D.; Petibon, R.; Hynes, T.; Liu, Q. Q.; Dahn, J. R. Studies of Gas Generation, Gas Consumption and Impedance Growth in Li-Ion Cells with Carbonate or Fluorinated Electrolytes Using the Pouch Bag Method. *J. Electrochem. Soc.* **2017**, *164* (2), A340−A347.
(168) Eshetu, G. G.; Grugeon, S.; Gachot, G.; Mathiron, D.; Armand, M.; Laruelle, S. LiFSI vs. LiPF6 Electrolytes in Contact with Lithiated Graphite: Comparing Thermal Stabilities and Identification of Specific SEI-Reinforcing Additives. *Electrochim. Acta* **2013**, *102*, 133−141.
(169) Hou, J.; Lu, L.; Wang, L.; Ohma, A.; Ren, D.; Feng, X.; Li, Y.; Li, Y.; Ootani, I.; Han, X.; Ren, W.; He, X.; Nitta, Y.; Ouyang, M. Thermal Runaway of Lithium-Ion Batteries Employing LiN(SO2F)2-Based Concentrated Electrolytes. *Nat. Commun.* **2020**, *11* (1), 1−11.
(170) Louli, A. J.; Eldesoky, A.; DeGooyer, J.; Coon, M.; Aiken, C. P.; Simunovic, Z.; Metzger, M.; Dahn, J. R. Different Positive Electrodes for Anode-Free Lithium Metal Cells. *J. Electrochem. Soc.* **2022**, *169* (4), No. 040517.
(171) Aiken, C. P.; Logan, E. R.; Eldesoky, A.; Hebecker, H.; Oxner, J. M.; Harlow, J. E.; Metzger, M.; Dahn, J. R. Li[Ni 0.5 Mn 0.3 Co 0.2]O 2 as a Superior Alternative to LiFePO 4 for Long-Lived Low Voltage Li-Ion Cells. *J. Electrochem. Soc.* **2022**, *169* (5), No. 050512.
(172) Koltypin, M.; Aurbach, D.; Nazar, L.; Ellis, B. On the Stability of LiFeP O4 Olivine Cathodes under Various Conditions (Electrolyte Solutions, Temperatures). *Electrochem. Solid-State Lett.* **2007**, *10* (2), A40−A44.
(173) Yang, L.; Deng, W.; Xu, W.; Tian, Y.; Wang, A.; Wang, B.; Zou, G.; Hou, H.; Deng, W.; Ji, X. Olivine LiMnxFe1−xPO4 Cathode Materials for Lithium Ion Batteries: Restricted Factors of Rate Performances. *J. Mater. Chem. A* **2021**, *9* (25), 14214−14232.

https://doi.org/10.1021/acsenergylett.3c01529
ACS Energy Lett. 2023, 8, 4572−4596